nature cell biology

Article

https://doi.org/10.1038/s41556-025-01763-1

NOX1 and NPY1R mark regional colon stem cell populations that serve as cancer origins in vivo

Received: 15 June 2024

Accepted: 5 August 2025

Published online: 2 September 2025

Check for updates

Maxime Gasnier[1], Tanysha Chi-Ying Chen[1,7], Swathi Yada[1,7], Sowmya Sagiraju[1,7], Yusuke Yoshikawa[2], Stefano Perna[3], Hui Yi Grace Lim[1], Bernett Lee[3,4,5] & Nick Barker[1,6]

Current colorectal cancer mouse models either lack colon specificity, limiting progression towards more advanced disease, or preclude evaluation of resident stem cells as cancer origins. Here we report the identification of NOX1 and NPY1R as cell-surface markers enriched in LGR5$^+$ stem cells predominantly within the caecum and exclusively within the middle and distal colorectum, respectively. Selective dysregulation of Wnt signalling in NOX1$^+$ or NPY1R$^+$ stem cells using *CreERT2* mouse lines drives colon cancer initiation, predominantly within the caecum and rectum respectively, establishing these stem cell populations as important sources of colon cancer. Selective conditional activation of Wnt signalling and oncogenic *Kras* in combination with loss of TRP53 in these stem cell compartments resulted in the development of advanced, invasive cancers. This study establishes *CreERT2* drivers as valuable tools for studying stem cell contributions to colon cancer.

The epithelial lining of the gastrointestinal tract is essential for completing food digestion and mediating the efficient absorption of nutrients while also providing critical barrier functions and innate immune defence against potentially harmful microbes. Its extremely harsh operating environment imposes an obligate requirement for constant renewal, driven by discrete populations of stem cells residing within specialized niches at the base of deep invaginations within the epithelium known as crypts[1]. The functional units of the small intestine comprise many millions of finger-like villi, each associated with several crypts that collectively supply the new functional epithelial lineages needed to replace the billions of cells being extruded at villus tips daily. In contrast, the lining of the more distal part of the gastrointestinal tract, the colon, comprises multiple crypts that supply new functional lineages to a contiguous layer of flat surface epithelium. The colon is organized into anatomically distinct regions comprising the caecum, which directly connects the small intestine, followed by proximal, middle and distal compartments that terminate in the rectum and anus. Subtle differences in the architecture, composition and renewal rates of the epithelia from different regions of the colon, together with marked variations in their resident microbiome reflect their functional specialization[2–4]. Although the functions of the different compartments of the colon are not fully understood, the caecum is thought to play a role in water and nutrient absorption, as well as being a major site of fermentation[5,6]. The ascending and transverse colons are thought to absorb the remaining water and nutrients, leading to stool compaction before the descending colon is reached. This latter

[1]A*STAR Institute of Molecular and Cell Biology, Agency for Science, Technology and Research, Singapore, Singapore. [2]Department of Surgery, Nerima General Hospital, Tokyo, Japan. [3]Centre for Biomedical Informatics, Lee Kong Chian School of Medicine, Nanyang Technological University, Singapore, Singapore. [4]A*STAR Infectious Diseases Labs, Agency for Science, Technology and Research, Singapore, Singapore. [5]A*STAR Singapore Immunology Network, Agency for Science, Technology and Research, Singapore, Singapore. [6]Department of Physiology, Yong Loo Lin School of Medicine, National University of Singapore, Singapore, Singapore. [7]These authors contributed equally: Tanysha Chi-Ying Chen, Swathi Yada, Sowmya Sagiraju.
e-mail: nicholas_barker@a-star.edu.sg

main role is to facilitate the movement of waste material towards the rectum. This tissue compartmentalization translates into different cancer susceptibilities and aetiologies, making colorectal cancer (CRC) a very heterogeneous disease[7].

Regular exposure of the colonic epithelium to biomechanical injury, together with an associated obligate high rate of intrinsic cell proliferation, confers an elevated lifetime susceptibility to cancer-causing mutations. Accordingly, CRC is currently the third most diagnosed and second most lethal cancer worldwide, with incidence rates still increasing in many developed countries due to diet and lifestyle changes[8]. To study and tackle the progression of this disease, the development of physiologically relevant mouse models of advanced colon cancer is of crucial importance. Adult stem cells are known to be major sources of cancer following oncogenic transformation. LGR5 marks resident stem cells throughout the gastrointestinal tract that are responsible for daily renewal of the epithelial lining[9]. Targeted in vivo dysregulation of the Wnt pathway in gastrointestinal tract stem cells using *Lgr5*-Cre drivers efficiently drives cancer formation within the mouse small intestine, identifying LGR5$^+$ stem cells as important cancer origins in this tissue[9,10]. However, the rapid lethality arising from the resulting intestinal tumour load prevents evaluation of LGR5$^+$ colon stem cells as cancer origins and precludes the development and study of more advanced colon tumours in this mouse model. Other CRC models targeting the large intestine have been developed over the years[11–16]. However, to our knowledge, none of the Cre drivers used specifically target the stem cell compartment, precluding the study of cancer originating from and fuelled by this cell population. Identifying markers that selectively enrich for regional colon stem cells and facilitate their selective transformation as an essential prerequisite to evaluating their role in driving cancer and to generate accurate in vivo models of advanced colon cancer would therefore offer clinically relevant mechanistic insights into colon cancer development and deliver valuable pre-clinical screening models.

In this Article, we perform comparative transcriptomics on LGR5$^+$ stem cell populations from different regions of the gastrointestinal tract using LGR5 reporter mouse models to identify and validate markers selectively enriched in LGR5$^+$ colon stem cells. We accordingly identify *Nox1* and *Npy1r* as being highly enriched in LGR5$^+$ colon stem cells in the mouse caecum and middle/distal colorectum, as well as the middle/distal colorectum respectively. Using the mouse models *Nox1*-2A-Cre recombinase fused with a tamoxifen-inducible estrogen receptor (CreERT2), *Nox1*-2A-enhanced green fluorescence protein (eGFP) and *Npy1r*-eGFP-internal ribosome entry site (IRES)-CreERT2, we confirmed by lineage tracing and organoid initiation assays that cells positive for NADPH oxidase 1 (NOX1$^+$) and neuropeptide Y receptor Y1 (NPY1R$^+$) are bona fide stem cells capable of self-renewal and differentiation into both absorptive and secretory cell lineages in the colon. Crucially, we demonstrate that the *Nox1*-2A-CreERT2 and *Npy1r*-eGFP-IRES-CreERT2 drivers are capable of selectively initiating cancer in different regions of the colon following Wnt pathway hyperactivation, with minimal to no transformation observed in the small intestine. These observations identify colon stem cells as major cells of cancer origin throughout the colon in mice. Importantly, we also demonstrate that combined activation of Wnt signalling, oncogenic Kras and loss of p53 function in these stem cell compartments results in the formation of more advanced, invasive cancers. These targeted Cre drivers will be invaluable for accurately modelling advanced cancer within different regions of the colon by incorporating prevalent mutations to deliver clinically relevant mechanistic insights into regional cancer progression.

Results

NOX1 selectively enriches for LGR5-expressing stem cells in the colon

To identify markers specifically enriched in colonic stem cells, we profiled the transcriptome of fluorescence-activated cell sorting (FACS)-isolated GFP^{high} and GFP^{neg} cell populations from the small intestine and colon of our non-variegated *Lgr5*-2A-eGFP reporter mice[17] (Fig. 1a). Comparison of their respective GFP^{high} and GFP^{neg} transcriptomes revealed the signature of the LGR5-expressing stem cells in each region. As expected, there was a significant overlap with the previous colon LGR5$^+$ stem cell signature generated using *Lgr5*-eGFP-IRES-CreERT2 reporter mice, including many Wnt target genes[18] (Extended Data Fig. 1a). The LGR5$^+$ stem cell signature in the colon overlapped with a published mouse CD44$^+$ colon stem cell signature[19], including validated stem cell markers such as achaete-scute family BHLH transcription factor 2 (ASCL2)[18] (Supplementary Table 1). We identified the transcriptional signature of GFP^{high} stem cells for each tissue by screening it against the corresponding GFP^{neg} cell population. We then screened the list of genes enriched in the colon GFP^{high} stem cells against the GFP^{high} stem cell transcriptional signature of the small intestine and pylorus[20] to identify genes selectively upregulated in colonic stem cells (Fig. 1b and Supplementary Table 2). One of the most highly upregulated targets was *Nox1*, which is known to be enriched in the distal gastrointestinal tract[21,22] (Fig. 1c). Nevertheless, a detailed characterization of the endogenous NOX1 expression pattern and functional evaluation of the stem potential of NOX1-expressing cells within the colon has not yet been performed.

NPY1R selectively enriches for LGR5-expressing stem cells in the middle and distal colon

To identify a more regionally restricted colon-specific stem cell marker, we conducted a new series of RNA sequencing (RNA-seq) analyses. Working with *Lgr5*-2A-eGFP mice, we separated the small intestine into three regions to mimic the anatomical separation of this tissue (that is, the duodenum, jejunum and ileum) and divided the colon into two regions (proximal and distal) (Fig. 1d). We then identified the gene signature for each region by comparing the GFP^{high} and GFP^{neg} transcriptomes (Supplementary Tables 3 and 4). Finally, we compared the list of genes enriched in the proximal or distal colon against the GFP^{high} stem cell transcriptional signature of the small intestine (all regions) and pylorus. We also compared the list of genes enriched in the distal colon against that of the proximal colon and vice versa to isolate a specific gene signature for each region of the colon (Fig. 1e and Supplementary Tables 5 and 6). Although we failed to validate via quantitative PCR (qPCR) and RNAscope a robustly expressed, selective marker of LGR5$^+$ stem cells in the proximal colon (Extended Data Fig. 1b and Supplementary Table 5), we identified *Npy1r* as one of the most highly enriched genes in the LGR5$^+$ population of the distal colon (Fig. 1f and Supplementary Table 6). NPY1R is known to be expressed in a subset of enteroendocrine cells in the gastrointestinal tract, but no stem cell enrichment has been described[23].

NOX1 is enriched in stem cell populations along the colon, whereas NPY1R is restricted to distal colon stem cells

To precisely define which lineages express NOX1 and NPY1R, we performed single-cell RNA-seq (scRNA-seq) on the epithelial fraction of the small intestine and colon. The small intestine was separated into three parts that were identical to the ones used for RNA-seq analysis (Fig. 1d). The colon was separated into four parts: the caecum and the proximal, middle and distal colon. Epithelial fractions were separated for each tissue the and cells were dissociated and embedded into chromium beads before RNA-seq. Using the shared nearest neighbour (SNN) modularity optimization-based clustering algorithm (implemented in Seurat), we identified 15, 14, 11 and 13 clusters for the caecum and proximal, middle and distal colon epithelium, respectively. Consensus lineage marker expression was plotted for each cluster of each tissue compartment (Fig. 2a) to assign clusters to their respective lineages (Fig. 2b). We then mapped LGR5, NOX1 and NPY1R expression distribution on uniform manifold approximation and projection (UMAP) plots generated for each tissue (Fig. 2c) against the stem cell clusters

https://doi.org/10.1038/s41556-025-01763-1

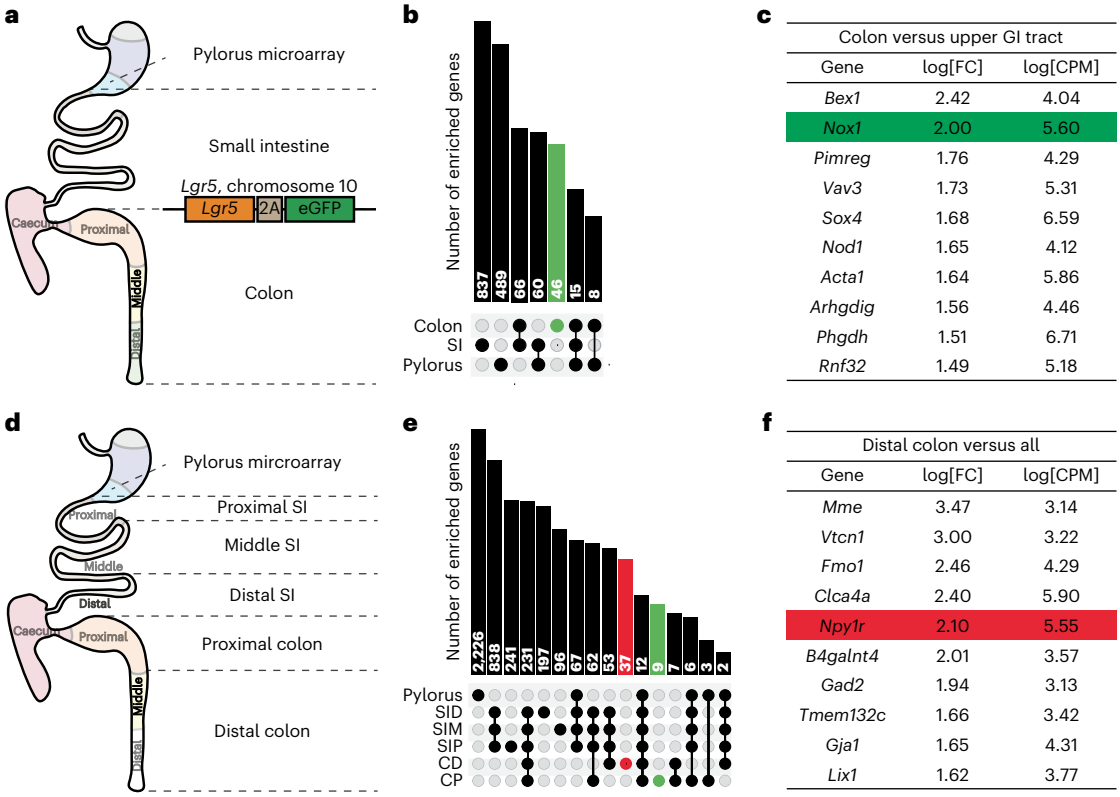

Fig. 1 | NOX1 and NPY1R are enriched in colon LGR5$^+$ cells. a, Single cells from *Lgr5*-2A-eGFP mouse colon and small intestine crypts were sorted by FACS according to their level of GFP expression. A published microarray performed in the pylorus using the *Lgr5*-eGFP-DTR mouse line (in which eGFP is fused to the diphtheria toxin receptor) was used as the pylorus stem cell transcriptomic signature[20]. From each tissue, GFP$^+$ and GFP$^-$ cell populations were collected for transcriptomic analysis. **b**, The LGR5$^+$ stem cell signature was generated by comparing the gene expression profiles of the GFP$^+$ and GFP$^-$ populations for each tissue. These lists of genes were then screened against both the small intestine and pylorus transcriptomic signatures. The UpSet plot represents the common enriched genes in LGR5$^+$ cells between tissues, as well as the enriched genes in LGR5$^+$ cells exclusive to each tissue (the enriched gene number for colonic LGR5$^+$ cells is highlighted in green). **c**, *Nox1* was identified as one of the most enriched genes in the colon stem cell compartment relative to all analysed upper gastrointestinal tract tissues (highlighted in green). **d**, Colon and small intestine tissues were separated into distinct anatomical parts (proximal, middle and distal small intestine and proximal and distal colon). An LGR5$^+$ stem cell signature was generated for each tissue using the same method as in **a**. **e**, UpSet plot representing the common enriched genes in LGR5$^+$ cells between tissues, as well as the enriched genes in LGR5$^+$ cells exclusive to each tissue (the distal colon only is highlighted in red and the proximal colon only is highlighted in green). **f**, *Npy1r* was identified as one of the most enriched genes in the distal colon stem cell compartment relative to all analysed upper gastrointestinal tract tissues (highlighted in red). CD, distal colon; CP, proximal colon; CPM, counts per million; FC, fold change; GI, gastrointestinal; SI, small intestine; SID, distal small intestine; SIM, middle small intestine; SIP, proximal small intestine.

delineated according to their assigned lineage identities (Fig. 2b). We found that NOX1 was expressed across many clusters at a very low level but highly upregulated within the stem cell cluster for all parts of the colonic epithelium (Fig. 2c), in line with our RNA-seq data. In contrast, NPY1R-expressing cells overlapped with the stem cell cluster specifically in the middle and distal colon regions, with a higher expression in the distal colon, but not in the caecum or proximal colon (Fig. 2c). As was previously shown[23], a subpopulation of NPY1R$^+$ cells was found in the chromogranin A (CHGA$^+$) enteroendocrine cell cluster of the colon (Fig. 2c and Extended Data Fig. 1c). Interestingly, we also found a subpopulation of NPY1R-expressing cells in the tuft cell cluster in the distal colon (Fig. 2c).

We quantified the total number of LGR5$^+$ cells for each cluster and their expression status with respect to NOX1 and NPY1R expression (Extended Data Fig. 1d). We found that in the caecum 75.75% of the LGR5$^+$ stem cells co-expressed NOX1. Surprisingly, NOX1 was found to be co-expressed in only 29.15% of LGR5$^+$ stem cells in the proximal colon. This percentage increased towards the middle and distal part of the colon, with 84.52 and 77.73% of LGR5$^+$ stem cells co-expressing NOX1, respectively (Extended Data Fig. 1d). When looking at NPY1R expression in LGR5$^+$ stem cells, we showed that the percentage of co-expression increased from the middle to the distal colon (27.61 and 62.28%, respectively) and that the majority of the LGR5$^+$ stem cells (52.73%) co-expressed both NOX1 and NPY1R (Extended Data Fig. 1d). When looking at NOX1$^+$ and NPY1R$^+$ cells for each cluster, we also found that the majority of these cells were within the stem cell cluster (Extended Data Fig. 1e,f). For the caecum, we found that 66.08% of NOX1$^+$ stem cells expressed LGR5. This percentage remained constant in the proximal colon (65.22%) and distal colon (67.06%), but decreased in the middle colon (42.62%) (Extended Data Fig. 1e). NPY1R$^+$ stem cells were found to be present predominantly in the distal colon, with most co-expressing LGR5 and NOX1 (Extended Data Fig. 1f). Overall, these data show that NOX1 is expressed in the stem cell compartment of the entire large intestine, with the highest overlap in the caecum and distal colon (Extended Data Fig. 1d,e), whereas NPY1R expression is highly restricted to the distal colon stem cell compartment (Extended Data Fig. 1d,f).

For our small intestine scRNA-seq dataset, we again used the SNN modularity optimization-based clustering algorithm to identify 14, 15 and 16 clusters for the proximal, middle and distal small intestine epithelium, respectively. We plotted the key lineage marker expression for each cluster of each region (Extended Data Fig. 2a) in order to assign each cluster to its respective lineage identity on a UMAP plot (Extended Data Fig. 2b). We found NOX1 expression to be distributed at extremely

https://doi.org/10.1038/s41556-025-01763-1

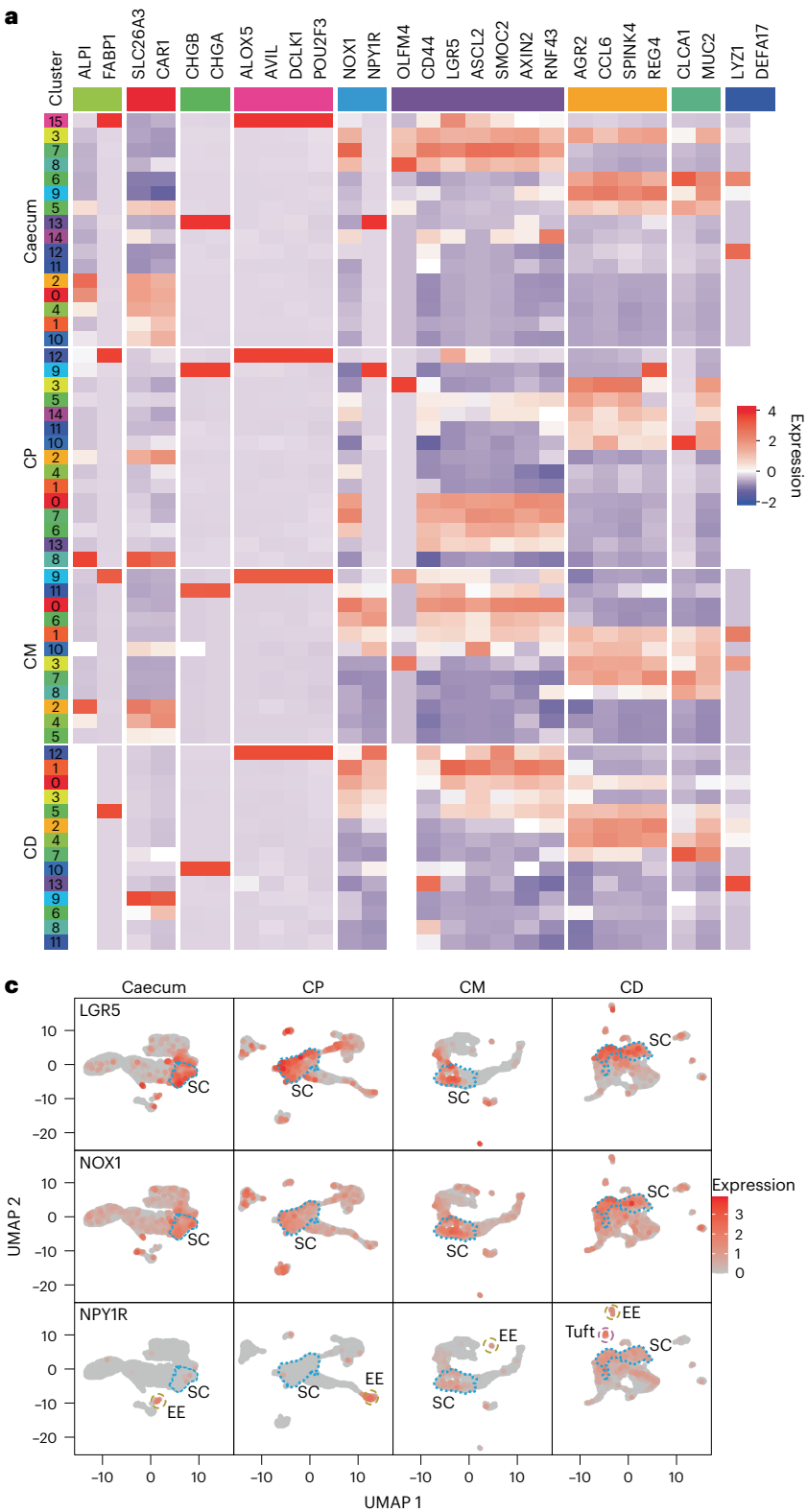

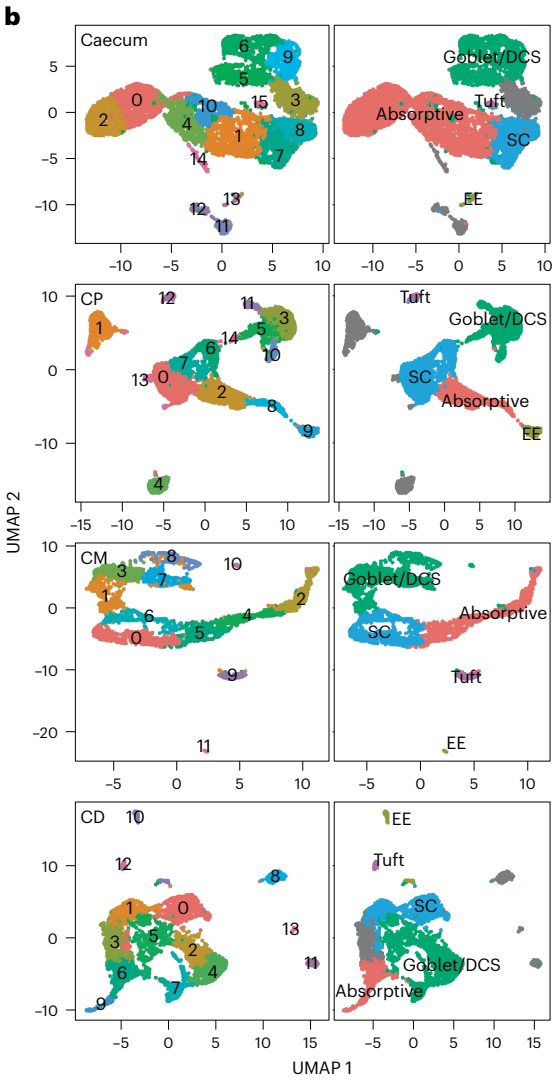

Fig. 2 | NOX1 and NPY1R are enriched in colon stem cell clusters. **a**, Heatmap representing the level of expression of identified key lineage markers for each cluster in the caecum and proximal, middle and distal colon. **b**, UMAP plots representing all of the clusters identified (left) before being reassigned to different lineage identities using the expression heatmap in **a** (right). **c**, UMAP plots representing the distribution of LGR5$^+$ (top), NOX1$^+$ (middle) and NPY1R$^+$ cells (bottom) for each colonic region (caecum and proximal, middle and distal colon). The stem cell (SC) cluster is delineated by a blue dotted line, the enteroendocrine (EE) cluster is delineated by a brown dashed line and the tuft cluster is delineated by a purple dashed line, according to the expression of consensus lineage markers as defined in **b**. Assays were performed on one biological sample per tissue region. CM, middle colon; DCS, deep crypt secretory.

https://doi.org/10.1038/s41556-025-01763-1

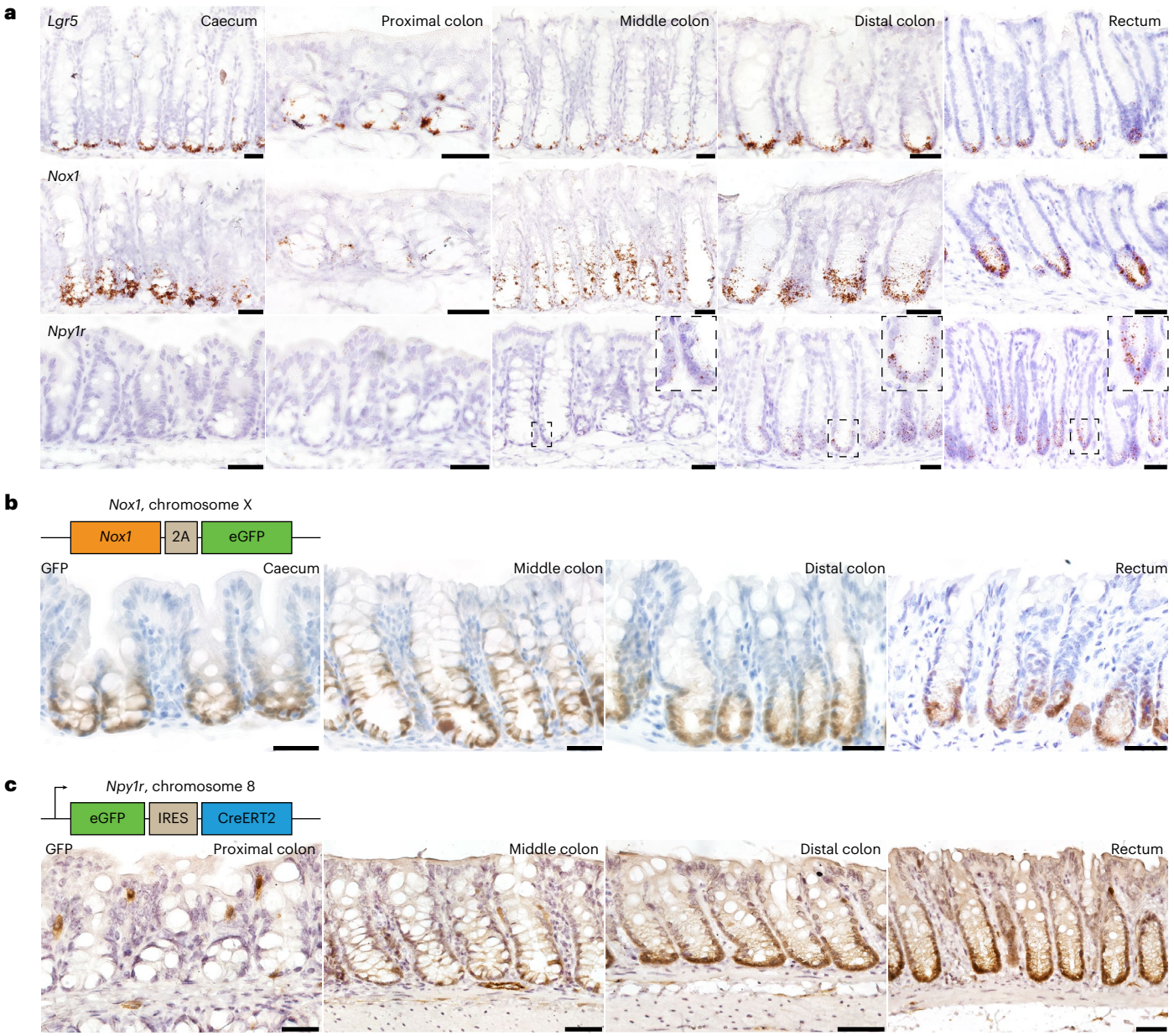

Fig. 3 | NOX1 and NPY1R are enriched at the base of colonic crypts. a, RNAscope analysis of *Lgr5*, *Nox1* and *Npy1r* in the different regions of the mouse colon, revealing enrichment of NOX1 and NPY1R at the crypt base of all compartments and the middle and distal colorectum, respectively ($n = 5$). **b**,**c**, *Nox1*-2A-eGFP ($n = 5$) (**b**) and *Npy1r*-eGFP-IRES-CreERT2 ($n = 5$) (**c**) mouse models were generated by incorporating the 2A-eGFP cassette before the stop codon at the *Nox1* gene locus and the eGFP-IRES-CreERT2 cassette after the start codon at the *Npy1r* gene locus. GFP IHC recapitulated endogenous NOX1 and NPY1R expression, as seen in **a**. GFP expression was also detected in the base of rectal crypts in *Npy1r* knock-in mice. Scale bars, 25 µm.

low, almost undetectable levels throughout all clusters of each part of the small intestine (Extended Data Fig. 2c). In contrast, we did not detect any NPY1R$^+$ cells in all regions of the small intestine except a subpopulation within the enteroendocrine cluster, which presented a very low level of NPY1R expression (Extended Data Fig. 2c). Taken together, these results demonstrate that NOX1 is expressed in stem cell compartments throughout the colon, with the highest enrichment present within the caecum and middle and distal regions. In contrast, NPY1R is selectively enriched in LGR5$^+$ stem cell compartments of the middle and distal colon, with the highest enrichment in distal regions.

Nox1 expression is restricted to crypt bases of the colon

Next, we validated our in silico transcriptomic analyses by first establishing endogenous *Nox1* RNA expression profiles within different regions of the colon using RNAscope. In the caecum and distal colorectum, the *Nox1* expression pattern was highly similar to that of *Lgr5*, with transcripts restricted to crypt bases (Fig. 3a). In the proximal colon, *Nox1* expression was similarly restricted to crypt bases but was only detected in a minority of crypts and at notably lower levels than *Lgr5* (Fig. 3a). In the middle colon, *Nox1* expression extended beyond the *Lgr5*$^+$ stem cell compartment at the crypt base to encompass presumptive early transit-amplifying cells (Fig. 3a).

Nox1 expression was largely absent from the stomach, duodenum and jejunum (Extended Data Fig. 3a), except for intestinal crypts directly adjacent to Peyer's patches, where expression was restricted to crypt bases (Extended Data Fig. 3b). Limited *Nox1* expression was also detected at crypt bases in the most distal part of the ileum, with robust expression present around the +4 to +6 positions immediately

adjacent to the Paneth cell compartment and low levels in a subset of crypt base columnar cells (Extended Data Fig. 3b).

Collectively, these expression analyses corroborate the in silico data, identifying *Nox1* as being highly and selectively expressed in *Lgr5*$^+$ epithelial stem cell compartments throughout the adult colon, with the greatest enrichment present within the caecum and distal colorectum.

Npy1r expression is restricted to crypt bases of the middle and distal colon

In contrast with *Nox1*, *Npy1r* expression was absent from the proximal colon and caecum of adult mice (Fig. 3a). In the middle colon, relatively weak *Npy1r* expression extended beyond the *Lgr5*$^+$ zone at the crypt base to encompass the lower third of the crypts in a pattern reminiscent of *Nox1* expression in this region (Fig. 3a). More robust levels of *Npy1r* were present exclusively within the *Lgr5*$^+$ zone at crypt bases throughout the distal colorectum (Fig. 3a). *Npy1r* expression was absent from epithelia of the small intestine, stomach and bladder, but exhibited robust levels in bladder stroma where *Npy1r* is known to mark a subset of fibroblast cells[24] (Extended Data Fig. 3c,d). Again, these expression analyses aligned well with our in silico data, identifying *Npy1r* as being highly enriched in *Lgr5*$^+$ epithelial stem cell compartments predominantly within the distal adult colorectum.

Nox1 and *Npy1r* knock-in mice faithfully report endogenous expression in the colon

To further characterize the various NOX1- and NPY1R-expressing colon populations, we generated independent eGFP reporter mouse models via targeted integration of either 2A-eGFP or eGFP-IRES-CreERT2 cassettes at the *Nox1* or *Npy1r* locus, respectively (Fig. 3b,c). GFP expression in adult *Nox1*-2A-eGFP reporter mice faithfully recapitulated endogenous NOX1 expression across all regions of the colon and ileum (Fig. 3b and Extended Data Fig. 4a). Similarly, GFP expression in *Npy1r*-eGFP-IRES-CreERT2 reporter mice was predominantly restricted to crypt bases of the middle and distal colorectum, recapitulating the endogenous expression pattern (Fig. 3c). Sporadic reporter expression was also observed scattered in stromal tissues throughout the colon and rectum (Fig. 3c) and bladder (Extended Data Fig. 4b).

Next, we sorted the GFP^{high} and GFP^{neg} cell populations from the different adult reporter mice by FACS to document the lineage identities of the NOX1$^+$ and NPY1R$^+$ colon populations using established markers via qPCR. For both NOX1-GFP^{high} and NPY1R-GFP^{high} cell populations, *Nox1* and *Npy1r*, respectively, together with *Lgr5* and the stem cell markers SPARC-related modular calcium-binding protein 2 (*Smoc2*)[25] and *Ascl2*, were robustly enriched compared with in GFP^{neg} populations (Extended Data Fig. 5a), further underscoring their relatively undifferentiated, stem-like identity. *Npy1r* was not enriched in the caecum, in line with our scRNA-seq and staining data (Extended Data Fig. 5a). Conversely, expression levels of the lineage markers downregulated in adenomas (*Dra*, also called *Slc26a3*—a colonocyte marker), *Mucin2* (*Muc2*—a goblet marker) and regenerating family member 4 (*Reg4*—a deep crypt secretory cell marker) were markedly lower in GFP^{high} compared with GFP^{neg} cell populations. The expression of *Chga* (an enteroendocrine marker) was also relatively low in NOX1$^+$ populations. In contrast, NPY1R$^+$ populations in the distal colon displayed robust *ChgA* expression (Extended Data Fig. 5a), consistent with observations from scRNA-seq analyses documenting the presence of enteroendocrine cells within this population (Fig. 2 and Extended Data Fig. 1c).

Co-immunofluorescence (co-IF) of GFP with CHGA, MUC2 and DRA across the different regions of the colon from adult NOX1 reporter mice confirmed a lack of co-localization with these mature lineage markers, further highlighting the relatively undifferentiated status of NOX1$^+$ populations (Extended Data Fig. 5b). NPY1R-GFP$^+$ colon populations similarly lacked co-expression of MUC2 or DRA markers, but did partially co-localize with CHGA, confirming that a subset of NPY1R$^+$ cells are enteroendocrine cells (Extended Data Fig. 5c). A subset of NOX1-GFP$^+$ and NPY1R-GFP$^+$ cells overlapped with the proliferation marker Ki-67, highlighting their proliferative status (Extended Data Fig. 5b,c).

NOX1$^+$ and NPY1R$^+$ cells establish long-term self-renewing colonic organoids in vitro

To evaluate the stem cell potential of NOX1-expressing colon cells, we FACS-sorted NOX1-GFP^{high} and NOX1-GFP^{neg} cells from the caecum and distal colon of adult *Nox1*-2A-eGFP reporter mice and assessed their capacity to form long-term organoid cultures in vitro (Fig. 4a). The organoid outgrowth efficacy of plated GFP^{high} cells relative to GFP^{neg} cells was 11-fold higher in the caecum and 5.5-fold higher for the distal colon (Fig. 4b). Importantly, the limited numbers of caecum and colon organoids generated from GFP^{neg} cells could not be maintained beyond the first passage, in contrast with GFP^{high} cell-derived organoids, which could be cultured long term (more than ten passages) (Fig. 4c).

We also FACS sorted NPY1R-GFP^{high} and NPY1R-GFP^{neg} cells from the distal colon of adult *Npy1r*-eGFP-IRES-CreERT2 reporter mice (Fig. 4d). The organoid outgrowth efficacy of plated GFP^{high} cells relative to GFP^{neg} cells was 5.5-fold higher (Fig. 4e). Again, the limited number of GFP^{neg} cell-derived organoids could not be maintained beyond the first passage, in contrast with the GFP^{high} cell-derived organoids that could be passaged long term (Fig. 4f).

To formally document the in vitro multipotency of the plated NOX1$^+$ and NPY1R$^+$ cells, we performed a differentiation assay. Organoids derived from either NOX1$^+$ or NPY1R$^+$ cells were cultured in growth

Fig. 4 | NOX1-expressing cells demonstrate stem cell potential in vitro. **a**, *Nox1*-2A-eGFP single cells from caecum and distal colon crypts were isolated by FACS according to their GFP expression level. The lines on the plot indicate the boundaries of the gates set for demarcating a GFP-neg and GFP-high population. The x-axis indicates that the GFP signal was measured by excitation with a 488 nm laser and emission collected by a 530/40 nm filter. **b**, Caecum ($n = 3$; 3.2633 ± 0.1335%) and colon ($n = 3$; 3.9233 ± 0.3398%) organoid outgrowth efficiencies were calculated as the number of organoids formed at passage 0 (P0) relative to the total number of cells seeded. Only GFP$^+$ cells had the potential to grow organoids. **c**, Representative images of newly established caecum (top) and distal colon organoids (bottom) at P0 and P10. GFP$^+$ cell-derived organoids were passaged for more than ten passages. **d**, *Npy1r*-eGFP-IRES-CreERT2 single cells from the distal colon were isolated by FACS according to their GFP expression level. The lines on the plot indicate the boundaries of the gates set for demarcating a GFP-neg, GFP-mid and GFP-high population. The x-axis indicates that the GFP signal was measured by excitation with a 488 nm laser and emission collected by a 530/40 nm filter. **e**, The distal colon organoid outgrowth efficiencies of GFP$^-$ and GFP$^+$ cells showed that only GFP$^+$ cells had the potential to grow organoids ($n = 6$; 5.6166 ± 0.8734%). **f**, Representative images of distal colon organoids at P0 and P10. GFP$^+$ cell-derived organoids were passaged for more than ten passages. **g**, Schematic of the organoid differentiation protocol used to culture Matrigel-seeded cells, first for 2 d in organoid growth medium (OGM) before switching to organoid differentiation medium (ODM) once the organoids had been established for 3 (distal colon) or 5 d (caecum). **h**,**i**, qPCR analysis of *Nox1*-2A-eGFP-derived caecum (**h**) and distal colon (**i**) organoids, showing a decrease in the expression of *Nox1* (caecum = 0.1253 ± 7.623 × 10^{-3}; colon = 0.02760 ± 6.952 × 10^{-4}) and *Lgr5* (caecum = 0.1336 ± 5.044 × 10^{-3}; colon = 0.03647 ± 9.903 × 10^{-4}) and an increase in the expression of the lineage markers *Dra* (caecum = 97.575 ± 15.55; colon = 7.020 ± 0,5976), *Muc2* (caecum = 3.3936 ± 0.1463; colon = 5.765 ± 0.5768) and *ChgA* (caecum = 4.073 ± 0.2047; colon = 5.147 ± 0.1707) after differentiation ($n = 3$). **j**, qPCR analysis of *Npy1r*-eGFP-IRES-CreERT2-derived distal colon organoids showing a decrease in the expression of *Lgr5* (0.112 ± 9.644 × 10^{-3}) and an increase in the expression of the lineage markers *Dra* (23.9223 ± 1.908), *Muc2* (2.8366 ± 0.1787) and *ChgA* (3.4676 ± 0.1252) after differentiation ($n = 3$). *Npy1r* expression was unchanged after differentiation (0.8083 ± 0.1501). Statistical significance in **b**, **e** and **h**–**j** was determined by two-tailed *t*-test and the data are presented as means ± s.e.m. Scale bars, 150 µm. FSC, forward scatter.

https://doi.org/10.1038/s41556-025-01763-1

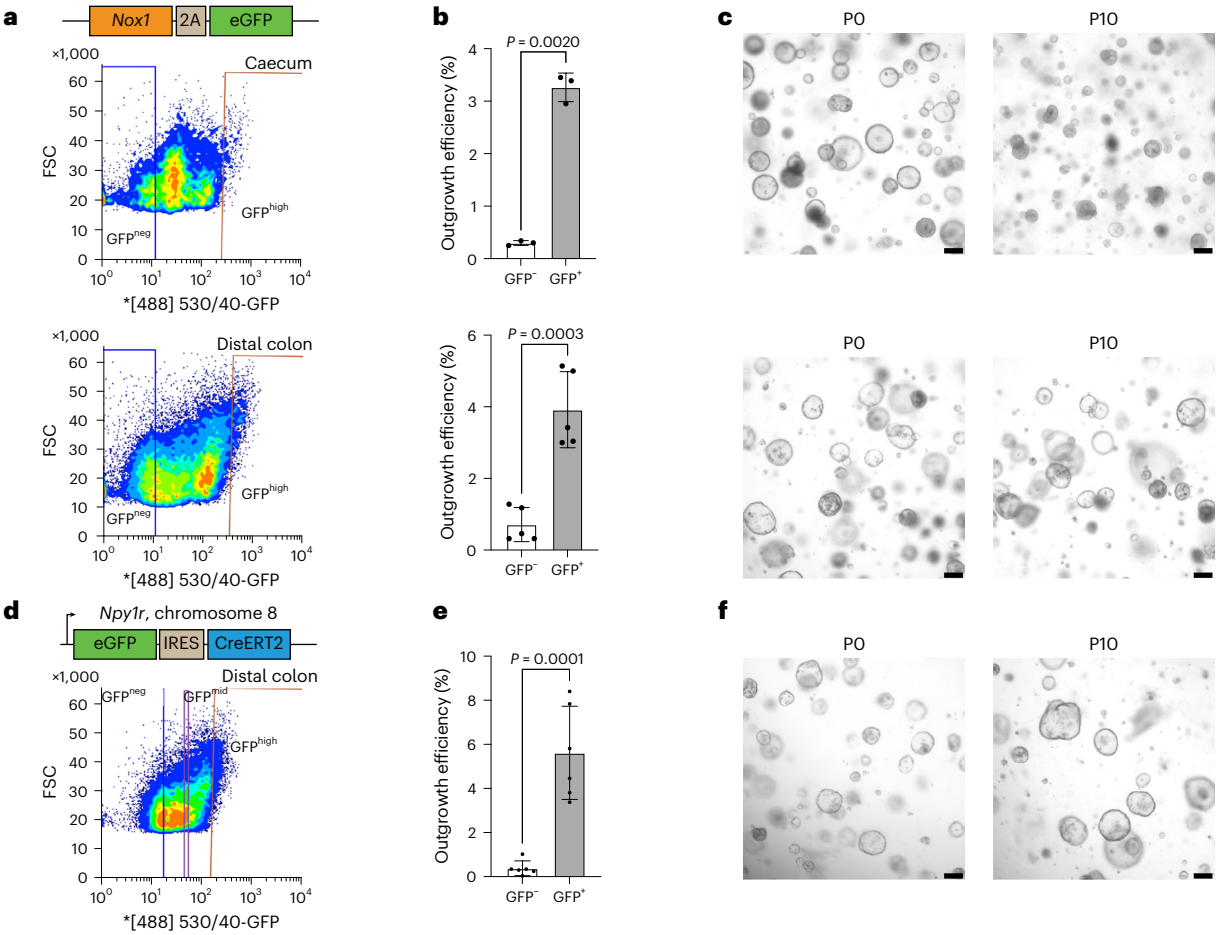

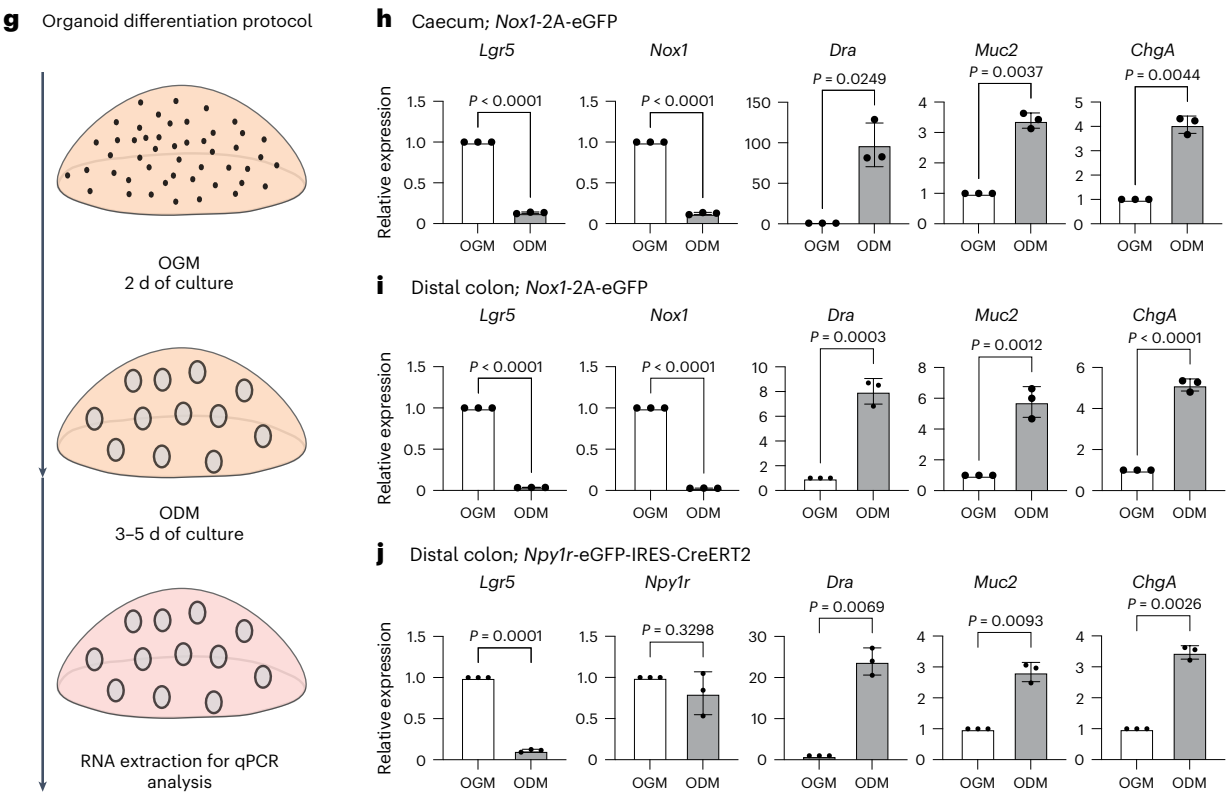

medium for 2 d before switching to a differentiation medium for 3 and 5 d for the distal colon and caecum, respectively (Fig. 4g). qPCR analyses on NOX1$^+$ cell-derived caecum and distal colon organoids documented a major decrease in both *Nox1* and *Lgr5* expression and a concomitant increase in differentiated lineage marker expression (Fig. 4h,i). NPY1R$^+$ cell-derived distal colon organoids similarly displayed a marked increase in differentiated lineage marker expression, with only a modest accompanying decrease in *Npy1r*, probably due to the presence of *Npy1r*-expressing enteroendocrine cells (Fig. 4j). Collectively these results identify NOX1$^+$ populations from both the caecum and distal colon and the NPY1R$^+$ population from the distal colon as being highly enriched for cells with robust stem cell potential in vitro.

NOX1 marks self-renewing, multipotent colon stem cell populations in vivo

To functionally evaluate the endogenous stem cell identity of NOX1-expressing cells within the adult colonic epithelium, we generated a *Nox1*-2A-CreERT2/*Rosa26*-tdTomato (tdTom) mouse model to track the contribution of endogenous NOX1-expressing cells to homeostatic epithelial renewal via in vivo lineage tracing (Fig. 5a). At 24 h after tamoxifen induction, cells at the base of the crypts of the colon expressed tdTom, with only a subset of labelled crypts in the proximal colon, recapitulating the expression profiles observed via RNAscope analyses and the eGFP reporter model (Fig. 5b). One week after induction, tdTom-labelled progeny had expanded to encompass most of the crypts (Fig. 5b). One month after tamoxifen induction, the vast majority of crypts and the associated surface epithelium in the caecum (97.7%), middle (91.7%) and distal colon (92.5%) and rectum (75%), together with scattered crypts in the proximal colon, were entirely tdTom positive (Fig. 5b and Extended Data Fig. 6a). Co-IF analyses of tdTom with major cell lineage markers confirmed overlapping expression in tracing units across all regions of the colon (Fig. 5c). Collectively, these observations identify NOX1$^+$ populations as harbouring self-renewing, multipotent stem cells contributing to epithelial homeostasis throughout the colon.

We further explored the clonal dynamics of lineage tracing using the *Nox1*-2A-CreERT2 driver by administering a low dose of tamoxifen (0.1 mg per 30 g bodyweight) to initiate recombination at low frequency. This tamoxifen dose is sufficient to activate tdTom expression within single cells at colonic crypt bases after 24 h in both the middle and distal colon (top panel of Extended Data Fig. 6b). As expected, tracing units initiated from these single NOX1$^+$ cells had expanded upwards from the crypt base after 1 week (middle panel of Extended Data Fig. 6b). A subset of the tracing units further expanded to encompass entire crypts by 1 month (bottom panel of Extended Data Fig. 6b), confirming that individual NOX1-expressing stem cells have the potential to populate entire colonic crypts during epithelial renewal. With this low level of induction, the proportion of crypts containing tdTom$^+$ cells rapidly decreased over time, from 95.66 ± 3.44 and 87.33 ± 6.15% of crypts at 24 h to 48.44 ± 14.37 and 44 ± 8.88% of crypts after 1 week and 31.11 ± 9.11 and 34.44 ± 7.40% of crypts after 1 month in the middle and distal colon, respectively (Extended Data Fig. 6c). The decreases in the number of tdTom$^+$ crypts 24 h and 1 month after induction in the middle and distal colon were statistically significant ($P < 0.0001$), probably reflecting known stem cell competition dynamics between labelled and non-labelled colonic stem cells in these crypts[26–28]. In contrast, using the same low tamoxifen dose, we found that a larger pool of NOX1-expressing cells were labelled at crypt bases of the caecum after 24 h (Extended Data Fig. 6b), resulting in a higher frequency of retained lineage tracing after 1 month (70.4 ± 10.98% tdTom$^+$ caecum crypts after 24 h and 61.33 ± 9% after 1 month; $P = 0.0674$) (Extended Data Fig. 6c). Thus, NOX1-expressing cells present distinct lineage tracing dynamics in different regions of the colon, with more efficient recombination and retention of clones within the caecum.

In the small intestine, long-term tracing was only observed in the distal ileum and crypts adjacent to the Peyer's patches (Extended Data Fig. 7a,b), in line with the endogenous NOX1 expression observed within the LGR5$^+$ stem cell compartments of those regions (Extended Data Figs. 3b and 4a). Following induction with 3 mg tamoxifen per 30 g bodyweight, lineage tracing in the ileum originated predominantly from presumptive early transit-amplifying cells immediately adjacent to the Paneth cell compartment, although tdTom expression was also observed in limited numbers of crypt base columnar cells interspersed with Paneth cells at the crypt base after 24 h (Extended Data Fig. 7a). Accordingly, limited numbers of tdTom$^+$ ribbons spanning crypt–villus units present in the distal ileum after 1 week were retained after 1 month (Extended Data Fig. 7a). In contrast, multiple tdTom$^+$ cells were observed at the base of crypts adjacent to Peyer's patches after 24 h (Extended Data Fig. 7b). After 1 week, tracing units had expanded along the entire crypt–villus axis and the follicle-associated surface epithelium (Extended Data Fig. 7b). By 1 month, tracing units had further expanded to completely encompass the Peyer's patch-associated crypt–villus epithelium and the follicle lining epithelium (Extended Data Fig. 7b). These data highlight *Nox1*-2A-CreERT2 as being a highly selective colonic stem cell driver that readily facilitates recombination throughout the colon, along with accompanying sporadic recombination within the ileum.

NPY1R marks self-renewing, multipotent distal colon stem cell populations in vivo

To evaluate the endogenous stem cell identity of NPY1R$^+$ colon cells, we performed in vivo lineage tracing using *Npy1r*-eGFP-IRES-CreERT2, tdTom mice under homeostatic conditions (Fig. 6a). Due to the relatively low endogenous expression levels of NPY1R in the colon, we increased the tamoxifen dose to 4 mg per 30 g bodyweight to ensure robust recombination levels. At 24 h post-induction, single tdTom$^+$ cells were visible at the crypt bases within the middle colon, whereas a higher recombination frequency was achieved throughout the distal colon and rectum, with multiple tdTom$^+$ cells present at most crypt bases (Fig. 6b). After 1 week, basal tdTom$^+$ tracing units had expanded to reach the surface epithelium in multiple crypts in both the middle and distal colon and rectum, albeit at a higher frequency within more distal and rectal regions (Fig. 6b). The tracing frequency in the distal colon and rectum was maintained after 1 month, with 74.8% of colon crypts and associated surface epithelium displaying uniform tdTom expression and 81.8% of rectum crypts retaining tdTom labelling. Completely traced crypts were also present in the middle colon at this time point, albeit at a reduced frequency (22.7%) reflecting the lower induction efficacy in this region (Fig. 6b and Extended Data Fig. 8a). As expected, recombination within the crypts of the proximal colon was exclusively initiated within infrequent presumptive enteroendocrine cells at 24 h, but this was not retained at later time points (Fig. 6b).

To formally document the multipotency of NPY1R$^+$ colon cells, we performed red fluorescent protein (RFP) co-IF with CHGA, DRA and MUC2. Each lineage marker could be detected within tdTom$^+$ tracing units present in the middle and distal colon, confirming that NPY1R$^+$ cells can generate the various functional lineages of the colonic epithelium (Fig. 6c). We therefore conclude that NPY1R$^+$ crypt-base-resident populations in the middle and distal colorectum are highly enriched for long-term self-renewing, multipotent cells contributing to homeostatic epithelial renewal.

We additionally performed lineage tracing in the bladder to assess the behaviour of resident NPY1R$^+$ populations. After 24 h induction, tdTom$^+$ cells were detected within the stroma of the epithelium. This labelling was retained over time after 1 week and 1 month of tracing, indicating that NPY1R marks long-lived stromal cells in the bladder (Extended Data Fig. 8b). We performed co-IF staining of RFP with lineage markers. RFP$^+$ cells failed to co-localize with the epithelium marker E-cadherin and the smooth muscle marker alpha smooth muscle actin. In contrast, RFP$^+$ cells were uniformly positive for the mesenchyme

https://doi.org/10.1038/s41556-025-01763-1

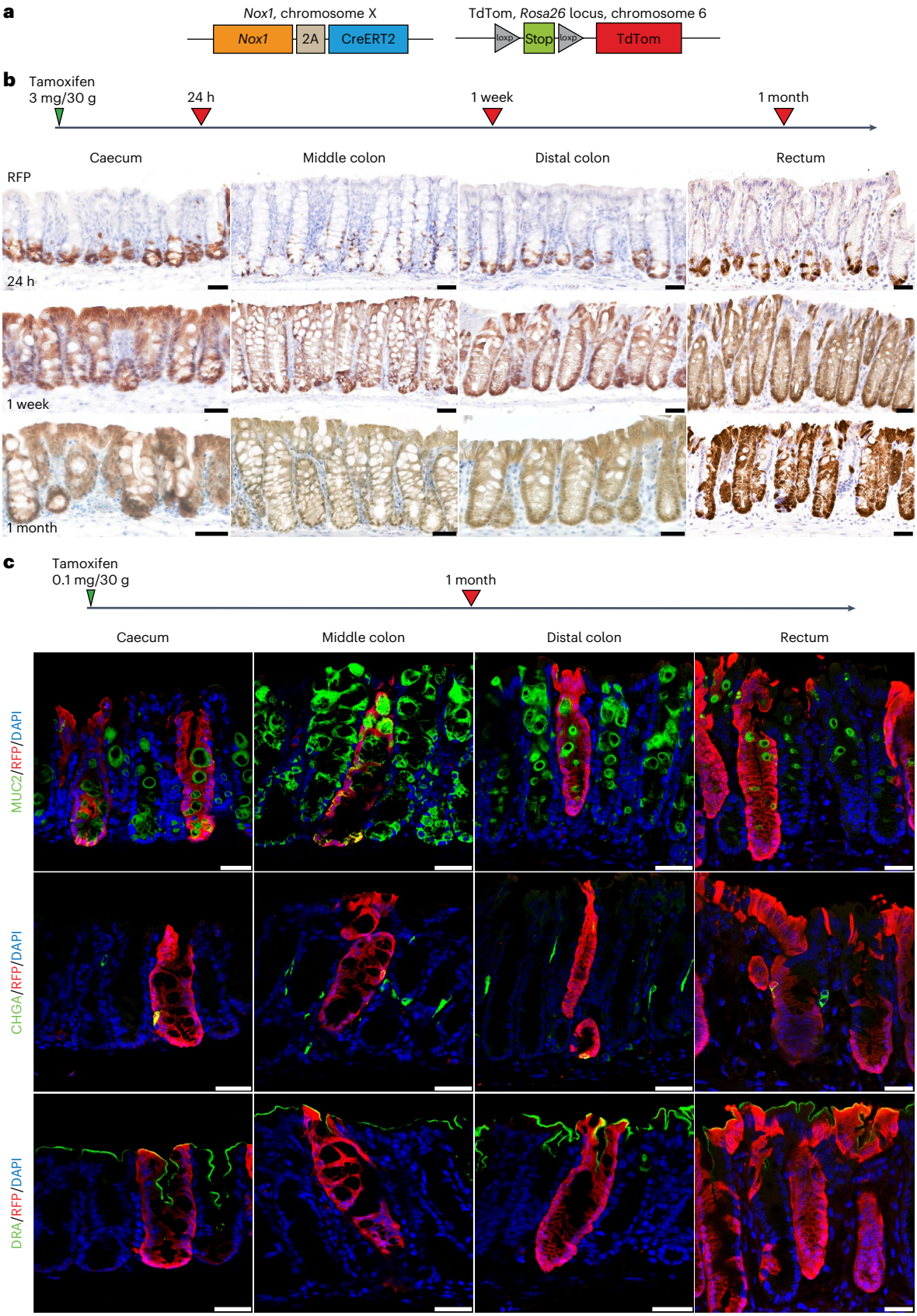

Fig. 5 | NOX1-expressing colon cells are self-renewing, multipotent stem cells in vivo. a, A *Nox1*-2A-CreERT2 mouse model was generated by incorporating the 2A-CreERT2 cassette before the stop codon at the *Nox1* gene locus. Mice were crossed with the *Rosa26*-LSL-tdTom mouse line. **b**, Mice were injected with 3 mg tamoxifen per 30 g body weight (3 mg/30 g) and analysed at 24 h ($n = 3$), 1 week ($n = 3$) and 1 month ($n = 3$) after induction. RFP IHC showed lineage tracing of NOX1-expressing cells and their cell progeny. **c**, Mice were injected at a lower tamoxifen dose (0.1 mg per 30 g body weight) and harvested at 1 month ($n = 3$). Co-IF of RFP and the lineage markers MUC2, CHGA and DRA showed that all RFP$^+$ traced units expressed major lineage markers. Scale bars, 25 µm.

https://doi.org/10.1038/s41556-025-01763-1

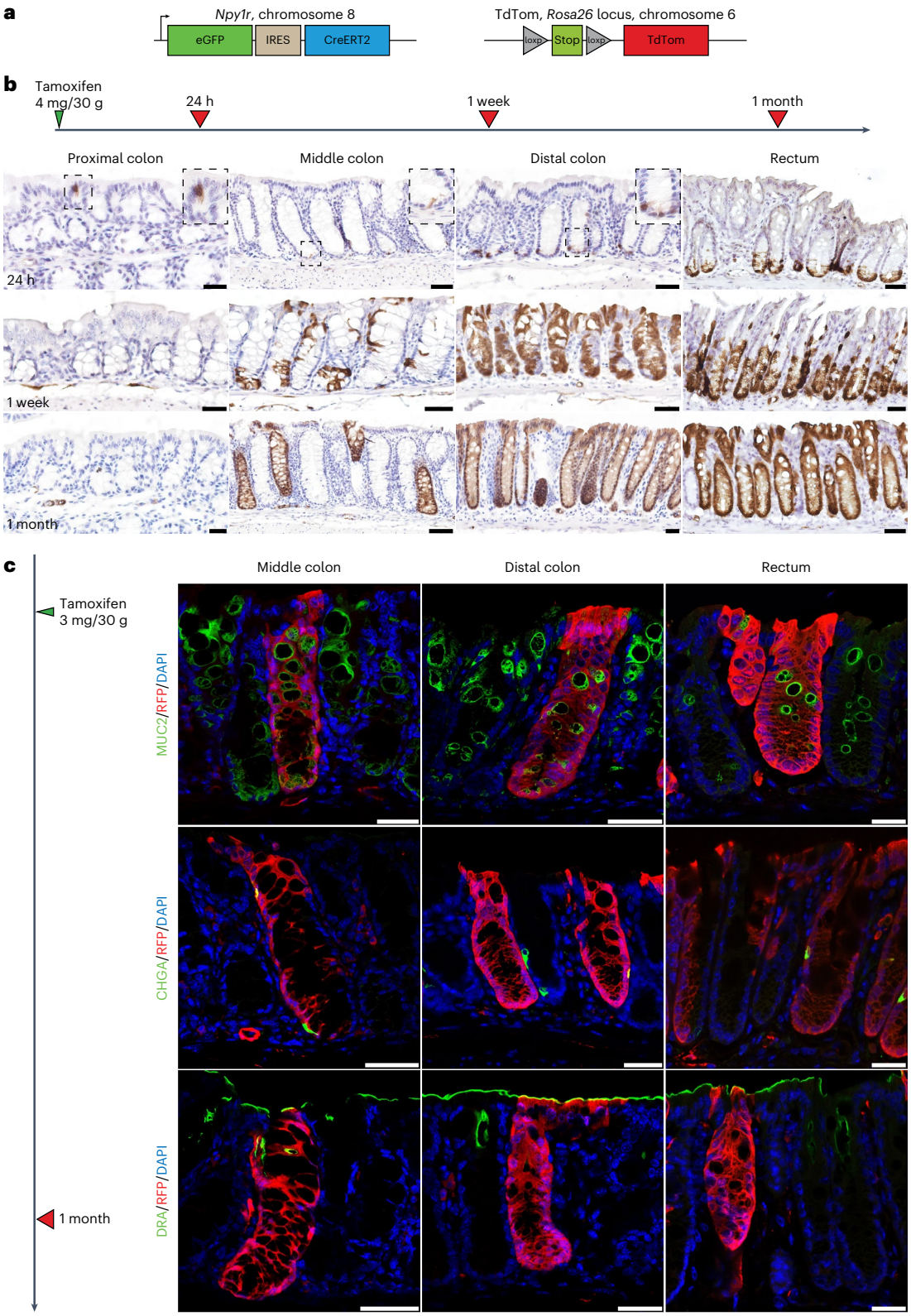

Fig. 6 | NPY1R-expressing colon cells are self-renewing, multipotent stem cells in vivo. a, *Npy1r*-eGFP-IRES-CreERT2 mice were bred with a *Rosa26*-LSL-tdTom mouse line. **b**, Mice were injected with 4 mg tamoxifen per 30 g bodyweight and harvested at 24 h ($n = 3$), 1 week ($n = 3$) or 1 month ($n = 3$) after injection. At 24 h, an RFP signal was detected in the epithelium of the proximal colon (see magnified insert). RFP was detected at the base of the crypt of the middle and distal colon, as well as the rectum. 1 week after induction, the RFP signal was lost in the proximal colon, whereas it spread from the base of the crypt in the middle and distal colon and the rectum. At 1 month, only the middle colon (at a lower frequency), distal colon and rectal crypts retained the RFP signal. **c**, Mice were injected with 3 mg tamoxifen per 30 g bodyweight and harvested after 1 month ($n = 3$). Co-IF of RFP and the lineage markers MUC2, CHGA and DRA showed that all RFP$^+$ traced units expressed major lineage markers. Scale bars, 25 µm.

marker vimentin, confirming the stromal identity of NPY1R$^+$ bladder cells (Extended Data Fig. 8c).

Targeted mutation of the genome of NOX1$^+$ stem cells drives cancer initiation predominantly in the caecum

LGR5$^+$ stem cells in the small intestine are major cells of cancer origin following targeted dysregulation of Wnt signalling in vivo using *Lgr5*-CreERT2 drivers[10]. The ensuing rapid tumour growth in the small intestine causes rapid lethality, precluding rigorous evaluation of LGR5$^+$ stem cell populations as cancer origins in the different regions of the colon. Having established the selective enrichment of NOX1 in stem cells within the caecum and middle and distal colon, we reasoned that the *Nox1*-2A-CreERT2 driver should facilitate selective targeting of oncogenic mutations to the genome of colon stem cells as an essential prerequisite to evaluating their role in driving colon cancer initiation. Hyperactivation of Wnt signalling via loss-of-function mutation of *APC* is a highly prevalent early event in human CRC[29]. We therefore generated a *Nox1*-2A-CreERT2;*Apc*$^{fl/fl}$ mouse model that incorporates a tdTom reporter allele to facilitate the visualization of any tumour formation in the gastrointestinal tract following targeted transformation of NOX1$^+$ stem cells (Fig. 7a). Non-induced adult mice were healthy, displayed very low levels of spontaneous recombination (as evidenced by <1 in 500 tdTom$^+$ colon crypts) and presented no evidence of Wnt pathway hyperactivation with the absence of β-catenin accumulation within all regions of the colonic epithelium (Extended Data Fig. 9a). One month after tamoxifen administration, nucleocytoplasmic accumulation of β-catenin (β-cat^{hi}) was apparent throughout the caecum and within discrete regions of the middle and distal colon (Fig. 7a). Co-IF for Ki-67 and β-catenin revealed that a subset of the β-cat^{hi} cells were actively proliferating in the different regions (Fig. 7b). Compared with control tissues, these Wnt-hyperactivated crypts were highly disorganized and displayed prominent signs of hyperplasia (Fig. 7a,b). In line with the higher efficiency of recombination within the caecum (Extended Data Fig. 6b,c), the caecum presented more polyps and a markedly higher proportion of crypts displaying nucleocytoplasmic β-catenin accumulation compared with crypts present in the middle and distal colon (Fig. 7a). To a lesser extent, we note an accumulation of β-catenin in the Peyer's patches of the small intestine within small proliferative cell clusters (Extended Data Fig. 9b,c). Crucially, unlike previous LGR5-driven cancer models in which small intestinal tumours rapidly develop[10], we did not detect any nucleocytoplasmic accumulation of β-catenin within the ileum, even after 1 month of induction (Extended Data Fig. 9b), highlighting the selectivity of the *Nox1*-2A-CreERT2 driver for initiating cancers within the colon as an essential prerequisite to modelling more advanced cancers in the caecum and distal colon via the incorporation of additional, physiologically relevant mutations.

Given the highly efficient recombination achieved in the caecum relative to the distal colon, we reasoned that reducing the tamoxifen induction dose would enable selective targeting of mutations affecting the caecum epithelium to facilitate the generation of a caecum-specific cancer model. As caecum cancer presents the highest rate of *Kras* mutation compared with other forms of CRC[30,31], we incorporated a conditional *Kras*^{G12D} allele into our *Nox1*-2A-CreERT2, *Apc*$^{fl/fl}$ mouse model (Fig. 7c). Following low dose tamoxifen induction of adult mice at 1 mg per 30 g bodyweight, we noted a major decrease of β-cat^{hi} polyps in the distal colon (one polyp was detected over four independent mouse colons), with no accompanying hyperactivation of phosphorylated MAPK (pMAPK). In contrast, the entire caecum epithelium harboured β-cat^{hi} polyps displaying robust hyperactivation of pMAPK, indicating a high recombination efficacy for both *Apc* and *Kras* alleles in the tissue (Fig. 7c). No β-cat^{hi} polyps were visible in the small intestine for both the ileum and Peyer's patches, and pMAPK activity was confined to the crypt base columnar cells and transit-amplifying compartment, as seen in non-induced mice (Extended Data Fig. 9d).

To further demonstrate the value of using the *Nox1*-2A-CreERT2 driver to generate more advanced cancers, we incorporated the conditional knockout mutant allele *p53*$^{fl/fl}$ into our model. We reasoned that incorporating a single floxed *Apc* allele to this compound mutant model would ensure a limited tumour load resulting from sporadic loss of heterozygosity of the second wild-type *Apc* allele, thereby ensuring a lifespan compatible with cancer progression, as previously shown[32]. Indeed, induction of the resulting *Nox1*-ATK mice resulted in the formation of an average of four to six large tumours in the caecum after 3 months, including advanced tumours independently characterized by a certified animal pathologist as being T2-stage adenocarcinomas undergoing robust invasion of the underlying submucosal layers. Immunohistochemistry (IHC) analyses confirmed successful recombination of the three conditional alleles in these tumours and loss of heterozygosity of *Apc*, as highlighted by β-catenin accumulation, pMAPK expression and loss of p53 expression (Fig. 7d). These results collectively identify NOX1$^+$ stem cells in the caecum and distal colon as key sources of cancer following in vivo mutation. Importantly, lower tamoxifen induction doses facilitate highly efficient targeting of conditional mutations affecting the caecum to selectively drive advanced cancer in this region.

Targeted mutation of the genome of NPY1R$^+$ stem cells drives cancer initiation in the distal colon

The well-established gene signature for distal CRC involves the sequential mutation of *Apc*, *Kras*, *Trp53* and *Smad4* alleles[33,34]. First, we incorporated the conditional *Apc*$^{fl/fl}$ and conditional *Kras*^{G12D} alleles by crossing with our *Npy1r*-eGFP-IRES-CreERT2, LoxP-Stop-LoxP (LSL)-tdTom mice (Fig. 8a). Non-induced mice showed no ectopic Cre activation in the colon (Extended Data Fig. 10a). Because of the low level of NPY1R expression, we increased the tamoxifen dosing regimen to three consecutive doses of 4 mg per 30 g bodyweight every 2 d. Due to the relatively slow growth of distal colon tumours compared with cancers originating in the caecum (Fig. 7b), mice were harvested at an extended timepoint of 8 weeks after induction to allow sufficient growth for detection. Nucleocytoplasmic accumulation of β-catenin was readily apparent only in the rectum, probably reflecting the relatively high levels of NPY1R-driven

Fig. 7 | NOX1-expressing stem cells serve as colon cancer origins following conditional mutation in vivo. a, The *Nox1*-2A-CreERT2 driver mouse line was crossed with the *Rosa26*-LSL-tdTom and *Apc*$^{fl/fl}$ mouse lines. Mice were bred to homozygosity. Mice were injected twice 2 d apart with 4 mg tamoxifen per 30 g bodyweight and harvested 1 month after injection ($n = 4$). β-catenin IHC showed nucleocytoplasmic accumulation in the caecum and middle and distal colon 1 month after induction. **b**, Co-IF for β-catenin and the proliferation marker Ki-67 showed hyperproliferation in the crypts of the caecum and middle and distal colon following *Apc* deletion ($n = 4$). **c**, *Nox1*-2A-CreERT2, *Apc*$^{fl/fl}$, *Rosa26*-LSL-tdTom mice were bred with the inducible LSL-*Kras*^{G12D} strain. LSL-*Kras*^{G12D} was kept heterozygotic. Mice were injected with 1 mg tamoxifen per 30 g bodyweight and harvested 1 month later ($n = 3$). β-catenin IHC showed nucleocytoplasmic accumulation throughout the caecum epithelium, with hyperactivation of Kras shown by an increase of pMapk. Only one polyp over four different colons was detected with nucleocytoplasmic β-catenin accumulation and pMapk hyperactivation. The rest of the colon presented with normal membranous β-catenin with no nucleocytoplasmic accumulation. **d**, A *p53*$^{fl/fl}$ allele was incorporated into the *Nox1*-2A-CreERT2, *Apc*$^{fl/+}$, LSL-*Kras*^{G12D} mouse model. Mice were injected with 2 mg tamoxifen per 30 g bodyweight and harvested 3 months after induction ($n = 4$). Tumours in the caecum presented with adenocarcinoma features with high levels of β-catenin accumulation, validating the loss of *Apc* heterozygosity. E-cadherin$^+$ cells had invaded the submucosa layer until the muscularis for the most advanced stage. Invading tumours were hyperactivated for KRAS (pMAPK$^+$) and devoid of p53 expression, highlighting efficient allelic recombination. Scale bars, 25 µm. D, day.

https://doi.org/10.1038/s41556-025-01763-1

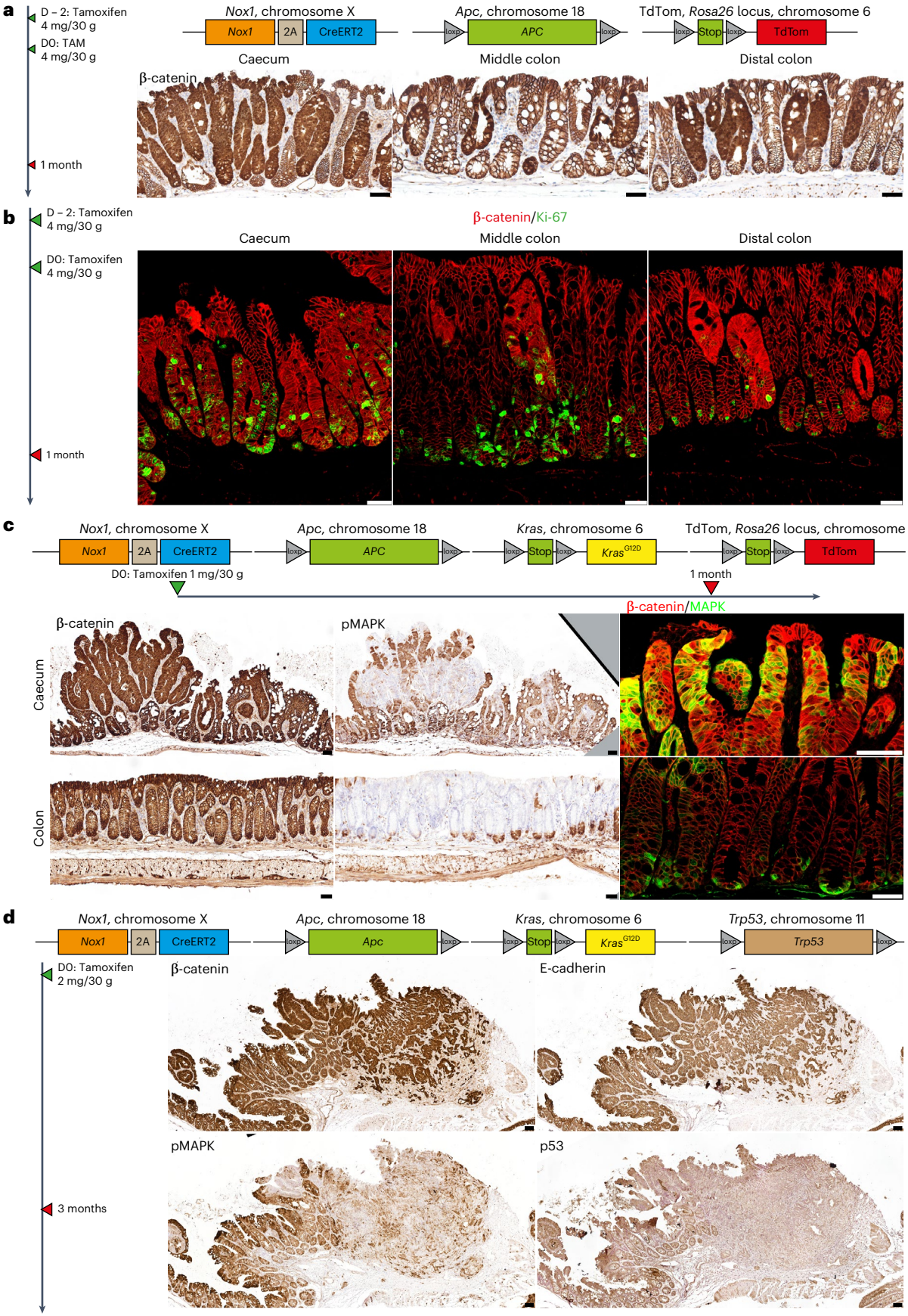

https://doi.org/10.1038/s41556-025-01763-1

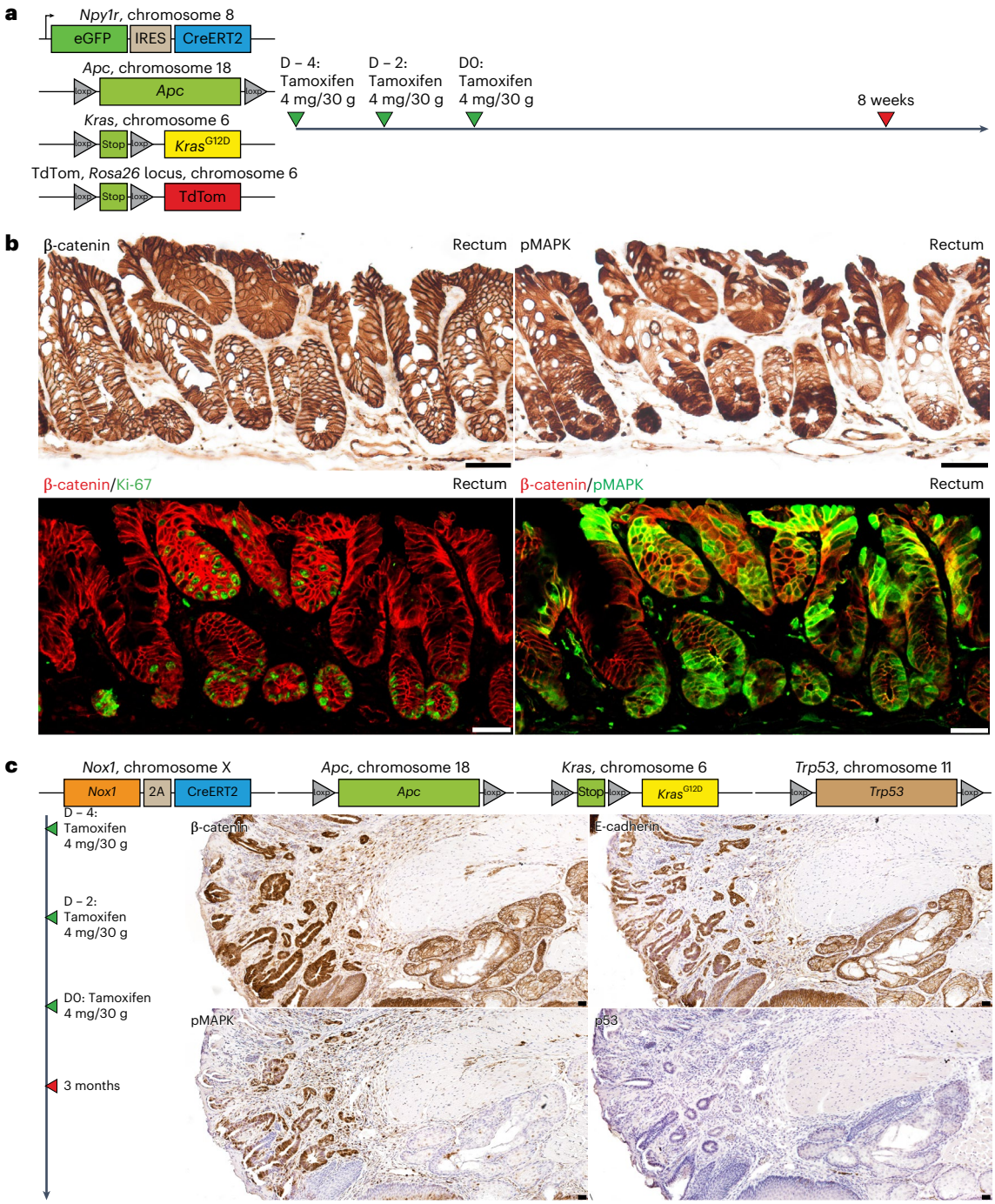

Fig. 8 | NPY1R-expressing stem cells serve as cancer origins in the distal colon following conditional mutation in vivo. a, The *Npy1r*-eGFP-IRES-CreERT2 driver mouse line was crossed with the *Rosa26*-LSL-tdTom, $Apc^{fl/fl}$ and LSL-$Kras^{G12D}$ mouse lines. Mice were bred to homozygosity and LSL-$Kras^{G12D}$ was kept heterozygotic. Mice were injected three times 2 d apart with 4 mg tamoxifen per 30 g bodyweight and harvested 8 weeks after injection ($n = 3$). **b**, β-catenin and pMAPK IHC showed localized nucleocytoplasmic accumulation in the rectum and pMAPK hyperactivation throughout the rectal epithelium. Co-IF for β-catenin and pMAPK showed co-localization of nucleocytoplasmic β-catenin and pMAPK hyperactivation. Co-IF for β-catenin and Ki-67 showed hyperproliferation in the crypts accumulating β-catenin following *Apc* deletion and *Kras* hyperactivation ($n = 3$). **c**, The $p53^{fl/fl}$ allele was incorporated into our mouse model. Mice were injected with three consecutive tamoxifen doses at 4 mg per 30 g body weight at 2-d intervals and harvested 3 months after induction ($n = 1$). Tumours presented with adenocarcinoma features, with β-catenin-accumulating E-cadherin$^+$ epithelial cells invading the subepithelial layer. These cells were hyperactivated for pMAPK and devoid of p53. Scale bars, 25 µm.

Cre expression levels in this region (Fig. 8b). pMAPK hyperactivation was detected throughout the entire rectum epithelium (Fig. 8b). Co-IF imaging of β-catenin and pMAPK showed that β-catenin-accumulating cells were hyperactivated for pMAPK (Fig. 8b). Co-IF imaging with the Ki-67 marker revealed that these Wnt-hyperactivated cells were highly proliferative (Fig. 8b). No β-catenin accumulation was observed in the bladder after 8 weeks of induction (Extended Data Fig. 10b).

Finally, we incorporated the $p53^{fl/fl}$ conditional knockout allele into the *Npy1r*-eGFP-IRES-$CreERT2^{hom}$, $Apc^{fl/fl}$, $Kras^{G12D/+}$ mouse model. *Npy1r*-eGFP-IRES-CreERT2 was used as a homozygote to ensure

sufficient Cre expression for the necessary multi-allelic recombination. Although the *Npy1r*-CreERT2 homozygote is effectively a knockout, *Npy1r*-knockout mice were healthy and fertile, as previously shown[35]. The colon was healthy and did not present any visible defects. At 3 months following tamoxifen induction, mice presented with a high tumour load in the rectal area with frequent rectal prolapses. Tumour features were independently characterized by a certified animal pathologist as adenocarcinomas displaying an onset of invasion through the submucosa layers (Fig. 8c). Thus, NPY1R$^+$ stem cells in the rectum serve as important sources of cancer formation following dysregulation of Wnt signalling in vivo. Incorporation of relevant compound conditional mutant alleles to the mouse validates the *Npy1r*-Cre driver as a powerful tool with which to model more advanced stages of rectal cancer originating from stem cells.

Discussion

In this study, we identify NOX1 and NPY1R as markers enriched in regionally distinct epithelial stem cell compartments within the colon. We demonstrate that NOX1$^+$ and NPY1R$^+$ cells are resident colonic stem cells that display properties of self-renewal and multipotency both in vivo and in vitro, expanding the limited toolkit of stem cell markers currently available for the study of this cell population. Indeed, colonic stem cells have to date been identified using the markers LGR5, SMOC2, ASCL2 and CD44, which also label the crypt base columnar stem cells of the small intestine, among other tissues[18,19,25]. Moreover, existing stem cell markers are expressed across all regions of the colon, greatly limiting their utility for identifying and characterizing the roles of diverse stem cell populations residing in tissue locations along the proximal-to-distal axis, which are known to have clear underlying differences in morphology, epithelial turnover and functions[2–4,7]. Our work therefore addresses this gap by identifying proximal (caecum)-enriched and distal-enriched colonic stem cell populations labelled, respectively, by NOX1 and NPY1R, allowing an in-depth evaluation of these region-specific populations in driving homeostasis, regeneration and disease.

We have previously employed *Lgr5*-CreERT2 mouse models to identify LGR5$^+$ stem cell populations in the small intestine as key cells of origin of Wnt-driven intestinal cancer[10]. However, the rapid lethality arising from the resulting tumour load in the small intestine precluded an evaluation of colon LGR5$^+$ stem cells as potential cancer origins using this model. Using colon-specific *Nox1*-2A-CreERT2 and *Npy1r*-eGFP-IRES-CreERT2 models that facilitate selective targeting of physiologically relevant conditional mutations to the genome of colon stem cells in the caecum or distal colorectum, respectively, we now formally document regional colon stem cell pools as important cancer origins. Crucially, by modulating the tamoxifen dosage administered to our NOX1 and NPY1R models and incorporating relevant sets of conditional mutant alleles known to drive human CRC, we can selectively initiate regional CRC formation that advances to invasive adenocarcinoma stages. These results highlight the potential of these stem cell Cre drivers for accurately modelling advanced CRC across different regions of the colon.

The value of such regional CRC models has emerged in part due to recent profiling efforts highlighting that colon cancer is a much more heterogeneous disease than was previously appreciated, with cancer aetiology, progression and treatment response dictated by their site of origin within the colon[36–38]. Indeed, the underlying mutation signatures differ markedly between proximal and distal colon cancers[30,31], and various factors, including the composition of the resident microbiome and local biomechanical inputs, are now recognized to influence cancer development and treatment responses[39,40]. At the same time, both caecum and rectal cancers present differing, yet highly debilitating, disease phenotypes and outcomes: caecum tumours are typically detected at advanced stages, accompanied by a high propensity for lymph node metastasis that ultimately results in poor prognosis[41,42], whereas rectum cancers, which account for 40% of all CRC cases, can be detected earlier but continue to reflect a high incidence and mortality[8], particularly in younger populations[43]. There is therefore an urgent need to develop more accurate CRC models that recapitulate intrinsic regional heterogeneities to deliver clinically relevant mechanistic insights that can underpin the development of more accurate diagnostic biomarkers and therapeutic targets in tackling this disease. We anticipate that our identification of NOX1 and NPY1R as region-specific colorectal stem cell markers, along with the generation of mouse models that can drive cancer initiation selectively in distinct regions of the colon, will serve as important pre-clinical models guiding these therapeutic efforts.

Online content

Any methods, additional references, Nature Portfolio reporting summaries, source data, extended data, supplementary information, acknowledgements, peer review information; details of author contributions and competing interests; and statements of data and code availability are available at https://doi.org/10.1038/s41556-025-01763-1.

References

1. Tan, D. W. & Barker, N. Intestinal stem cells and their defining niche. *Curr. Top. Dev. Biol.* **107**, 77–107 (2014).
2. Kiela, P. R. & Ghishan, F. K. Physiology of intestinal absorption and secretion. *Best. Pract. Res. Clin. Gastroenterol.* **30**, 145–159 (2016).
3. Martinez-Guryn, K., Leone, V. & Chang, E. B. Regional diversity of the gastrointestinal microbiome. *Cell Host Microbe* **26**, 314–324 (2019).
4. Hall, C., Youngs, D. & Keighley, M. R. Crypt cell production rates at various sites around the colon in Wistar rats and humans. *Gut* **33**, 1528–1531 (1992).
5. Brown, K., Abbott, D. W., Uwiera, R. R. E. & Inglis, G. D. Removal of the cecum affects intestinal fermentation, enteric bacterial community structure, and acute colitis in mice. *Gut Microbes* **9**, 218–235 (2018).
6. Den Besten, G. et al. The role of short-chain fatty acids in the interplay between diet, gut microbiota, and host energy metabolism. *J. Lipid Res.* **54**, 2325–2340 (2013).
7. Imperial, R. et al. Comparative proteogenomic analysis of right-sided colon cancer, left-sided colon cancer and rectal cancer reveals distinct mutational profiles. *Mol. Cancer* **17**, 177 (2018).
8. Xi, Y. & Xu, P. Global colorectal cancer burden in 2020 and projections to 2040. *Transl. Oncol.* **14**, 101174 (2021).
9. Barker, N. et al. Identification of stem cells in small intestine and colon by marker gene *Lgr5*. *Nature* **449**, 1003–1007 (2007).
10. Barker, N. et al. Crypt stem cells as the cells-of-origin of intestinal cancer. *Nature* **457**, 608–611 (2009).
11. Akyol, A. et al. Generating somatic mosaicism with a Cre recombinase–microsatellite sequence transgene. *Nat. Methods* **5**, 231–233 (2008).
12. Boutin, A. T. et al. Oncogenic *Kras* drives invasion and maintains metastases in colorectal cancer. *Genes Dev.* **31**, 370–382 (2017).
13. Kawaguchi, Y. et al. Mouse model of proximal colon-specific tumorigenesis driven by microsatellite instability-induced *Cre*-mediated inactivation of *Apc* and activation of *Kras*. *J. Gastroenterol.* **51**, 447–457 (2016).
14. Roper, J. et al. In vivo genome editing and organoid transplantation models of colorectal cancer and metastasis. *Nat. Biotechnol.* **35**, 569–576 (2017).
15. Tetteh, P. W. et al. Generation of an inducible colon-specific Cre enzyme mouse line for colon cancer research. *Proc. Natl Acad. Sci. USA* **113**, 11859–11864 (2016).
16. Xue, Y., Johnson, R., Desmet, M., Snyder, P. W. & Fleet, J. C. Generation of a transgenic mouse for colorectal cancer research with intestinal Cre expression limited to the large intestine. *Mol. Cancer Res.* **8**, 1095–1104 (2010).

17. Seishima, R. et al. Neonatal Wnt-dependent Lgr5 positive stem cells are essential for uterine gland development. *Nat. Commun.* **10**, 5378 (2019).
18. Van der Flier, L. G. et al. Transcription factor achaete scute-like 2 controls intestinal stem cell fate. *Cell* **136**, 903–912 (2009).
19. Habowski, A. N. et al. Transcriptomic and proteomic signatures of stemness and differentiation in the colon crypt. *Commun. Biol.* **3**, 453 (2020).
20. Tan, S. H. et al. AQP5 enriches for stem cells and cancer origins in the distal stomach. *Nature* **578**, 437–443 (2020).
21. Suh, Y. A. et al. Cell transformation by the superoxide-generating oxidase Mox1. *Nature* **401**, 79–82 (1999).
22. Van der Post, S., Birchenough, G. M. H. & Held, J. M. NOX1-dependent redox signaling potentiates colonic stem cell proliferation to adapt to the intestinal microbiota by linking EGFR and TLR activation. *Cell Rep.* **35**, 108949 (2021).
23. Hayashi, M. et al. Enteroendocrine cell lineages that differentially control feeding and gut motility. *eLife* **12**, e78512 (2023).
24. Baker, D. et al. A cellular reference resource for the mouse urinary bladder. Preprint at *bioRxiv* https://doi.org/10.1101/2021.09.20.461121 (2021).
25. Munoz, J. et al. The Lgr5 intestinal stem cell signature: robust expression of proposed quiescent '+4' cell markers. *EMBO J.* **31**, 3079–3091 (2012).
26. Azkanaz, M. et al. Retrograde movements determine effective stem cell numbers in the intestine. *Nature* **607**, 548–554 (2022).
27. Corominas-Murtra, B. et al. Stem cell lineage survival as a noisy competition for niche access. *Proc. Natl Acad. Sci. USA* **117**, 16969–16975 (2020).
28. Ritsma, L. et al. Intestinal crypt homeostasis revealed at single-stem-cell level by in vivo live imaging. *Nature* **507**, 362–365 (2014).
29. Zhan, T., Rindtorff, N. & Boutros, M. Wnt signaling in cancer. *Oncogene* **36**, 1461–1473 (2017).
30. Loree, J. M. et al. Classifying colorectal cancer by tumor location rather than sidedness highlights a continuum in mutation profiles and consensus molecular subtypes. *Clin. Cancer Res.* **24**, 1062–1072 (2018).
31. Yamauchi, M. et al. Assessment of colorectal cancer molecular features along bowel subsites challenges the conception of distinct dichotomy of proximal versus distal colorectum. *Gut* **61**, 847–854 (2012).
32. Fatehullah, A. et al. A tumour-resident Lgr5^{+} stem-cell-like pool drives the establishment and progression of advanced gastric cancers. *Nat. Cell Biol.* **23**, 1299–1313 (2021).
33. Fearon, E. R. & Vogelstein, B. A genetic model for colorectal tumorigenesis. *Cell* **61**, 759–767 (1990).
34. Vogelstein, B. et al. Genetic alterations during colorectal-tumor development. *N. Engl. J. Med.* **319**, 525–532 (1988).
35. Pedrazzini, T. et al. Cardiovascular response, feeding behavior and locomotor activity in mice lacking the NPY Y1 receptor. *Nat. Med.* **4**, 722–726 (1998).
36. Gallois, C., Pernot, S., Zaanan, A. & Taieb, J. Colorectal cancer: why does side matter? *Drugs* **78**, 789–798 (2018).
37. Hossain, M. S. et al. Colorectal cancer: a review of carcinogenesis, global epidemiology, current challenges, risk factors, preventive and treatment strategies. *Cancers (Basel)* **14**, 1732 (2022).
38. Xie, X. et al. Differences between carcinoma of the cecum and ascending colon: evidence based on clinical and embryological data. *Int. J. Oncol.* **53**, 87–98 (2018).
39. Wong, C. C. & Yu, J. Gut microbiota in colorectal cancer development and therapy. *Nat. Rev. Clin. Oncol.* **20**, 429–452 (2023).
40. Bras, M. M., Sousa, S. R., Carneiro, F., Radmacher, M. & Granja, P. L. Mechanobiology of colorectal cancer. *Cancers (Basel)* **14**, 1945 (2022).
41. Xie, Y. et al. Impact of tumor site on lymph node status and survival in colon cancer. *J. Cancer* **10**, 2376–2383 (2019).
42. Song, S., Wang, J., Zhou, H., Wang, W. & Kong, D. Poorer survival in patients with cecum cancer compared with sigmoid colon cancer. *Med. (Kaunas)* **59**, 45 (2022).
43. Bailey, C. E. et al. Increasing disparities in the age-related incidences of colon and rectal cancers in the United States, 1975–2010. *JAMA Surg.* **150**, 17–22 (2015).

Methods

Mice

Mouse lines. For *Nox1*-2A-eGFP and *Nox1*-2A-CreERT2, the cassettes were inserted immediately before the stop codon of the *Nox1* gene locus by homologous recombination in embryonic stem cells, thereby preserving the intact protein-coding region and endogenous expression of the genes. For *Npy1r*-eGFP-IRES-CreERT2, the cassettes were inserted immediately after the start codon of the *Npy1r* gene locus by homologous recombination in embryonic stem cells, thus eGFP and CreERT2 expression was under the direct control of the *Npy1r* locus promoter. *Rosa26*-LSL-tdTom (Ai14) (007914; The Jackson Laboratory) and LSL-*Kras*^{G12D} (019104; The Jackson Laboratory) mice were obtained from The Jackson Laboratory. *Lgr5*-2A-eGFP[17], *Apc*$^{fl/fl}$ (1857966; Mouse Genome Informatics)[44] and *Trp53*$^{fl/fl}$ (ref. 45) mice have been described previously. All of the lines were bred as homozygotes in a C57Bl/6J background. All mouse experiments were approved by the Institutional Animal Care and Use Committee of the Agency for Science, Technology and Research (A*STAR; 231777) and performed in compliance with all of the relevant ethical regulations. All animals were placed under a 12 h light/12 h dark cycle. The room temperature was maintained at 21 ± 1 °C with 55–70% humidity. All mice were bred and maintained under specific-pathogen-free conditions in individually ventilated cages. The maximum tumour size allowed by the Institutional Animal Care and Use Committee is 15 mm in any dimension and none of the experiments exceeded this limit. For all of the experiments, adult mice (not selected for sex, except for the FACS experiments) of a minimum age of 6–8 weeks were used.

Tamoxifen induction. Adult mice aged 6–12 weeks were induced with a single or double intraperitoneal injection of 3.3–133 mg tamoxifen per kg bodyweight (Sigma–Aldrich) dissolved in corn oil. Double and triple injections were performed at 2-d intervals.

Tissue collection. Mice were euthanized by carbon dioxide asphyxiation before tissue collection. The peritoneal cavity was opened with scissors and the connective tissue was removed from the organs using blunt forceps. The small intestine and colon were flushed with cold Hanks' Balanced Salt Solution (HBSS; Gibco). All of the organs were cut open longitudinally and the remaining faeces were removed by washing in HBSS.

Tissue fixation. Organs were incubated overnight at 4 °C (for immunochemistry or immunofluorescence) or 24 h at room temperature (for RNAscope) in 4% paraformaldehyde (Electron Microscopy Sciences) in phosphate-buffered saline (PBS) (wt/vol). For tissue processing in the RNAscope experiments, all tools were carefully cleaned with RNaseZap (Invitrogen) to prevent RNA degradation.

Crypt isolation and cell sorting

Mouse small intestine, colorectal or caecum tissues were incubated in chelation buffer (5.6 mM sodium phosphate, 8 mM potassium phosphate, 96.2 mM sodium chloride, 1.6 mM potassium chloride, 43.4 mM sucrose and 54.9 mM D-sorbitol in Milli-Q water) with 10 mM (colorectum and caecum) or 2 mM (small intestine) ethylenediaminetetraacetic acid (EDTA), 1 mM dithiothreitol and 1 mM *N*-acetylcysteine for 2 h (colorectum and caecum) or 45 min (small intestine) at 4 °C on a roller. Crypts were isolated by repeated pipetting of finely chopped tissue in cold chelation buffer. Chelation buffer containing isolated crypts was filtered through a 100-µm filter mesh and centrifuged at 720*g* at 4 °C for 3 min. The pellet was resuspended in TrypLE (Life Technologies) with DNase I (0.8 U µl^{-1}) (Sigma–Aldrich) and incubated at 37 °C for 10 min with intermittent trituration for digestion into single cells. Digestion was quenched by dilution with cold HBSS buffer. The suspension was centrifuged at 720*g* at 4 °C for 3 min. The pellet was resuspended in 2% foetal bovine serum (colorectum and caecum) or 20% foetal bovine serum + 5 mM EDTA and filtered through the 4-µm filter mesh cap of the FACS tube. Before sorting, 4′,6-diamidino-2-phenylindole (DAPI) was added at a final concentration of 1 µg ml^{-1} to stain dead cells. Single cells were sorted on a BD Influx Cell Sorter (BD Biosciences). Cells were collected in RLT Plus buffer (Qiagen) supplemented with β-mercaptoethanol (1/100) for RNA extraction, or advanced DMEM:F-12 medium (Gibco) supplemented with 0.5% Matrigel (Corning) for organoid culture.

RNA-seq and transcriptomic comparison

Single LGR5-GFP^{high} and -GFP^{neg} small intestinal or colonic epithelial cells from *Lgr5*-2A-eGFP mice were isolated by FACS (as described in the section 'Crypt isolation and cell sorting') and collected in RLT Plus + β-mercaptoethanol (1/100). A minimum of 30,000 cells for the colon and 50,000 cells for the small intestine were collected from each GFP fraction. Total RNA extracted from each fraction using the RNeasy Micro kit (Qiagen) was dissolved in RNase-free water and sent for sequencing at Novogene in Singapore. FASTQ files containing the RNA-seq reads were checked for quality control issues using FASTQC and MultiQC for which no issues were found. The reads were then mapped to the mouse genome build mm10 using STAR based on GENCODE M22 annotations. Gene counts were counted using featureCounts (part of the Subread package) based on GENCODE M22 annotations. The gene counts were then used in edgeR for a differential expression of genes analysis with multiple testing correction done using the Benjamini–Hochberg method.

Single-cell RNA-seq and analysis

10x Genomics scRNA-seq data were obtained as FASTQ files, which were processed with Cell Ranger version 7.1.0 using the mouse mm10 annotations for each individual tissue. For each tissue, the cell gene counts were imported into Seurat for independent data analysis. Cells were filtered to ensure that the number of detected genes was greater than 1,000 and the mitochondrial percentage was less than 20%. The top 2,000 variable features of the log-normalized counts data were used for principal component analysis. The top ten principal components (determined via an elbow plot) were then used to generate the SNN group, from which clusters were determined at a resolution of 0.5. Marker genes for each of the clusters were determined using the FindAllMarkers function in the Seurat package. These marker genes were then manually annotated to identify the various cell types. UMAP was performed on the top ten components to visualize the data. All analyses and visualizations were conducted in R version 4.2.1.

Organoid culture

FACS-isolated single cells were resuspended in growth factor-reduced Matrigel, seeded in 48-well plates and cultured in IntestiCult organoid growth medium (Stem Cell Technologies) supplemented with 20% Afamin/Wnt3a CM (MBL Life Science) and 100–200 µg ml^{-1} primocin (Invivogen), plus 10 µM Y-27632 (Sigma–Aldrich) for the first 2 d to prevent anoikis. Caecum organoid medium was supplemented with 100 ng ml^{-1} recombinant fibroblast growth factor 10 (PeproTech). The medium was refreshed every 2–3 d. Organoids were passaged when confluent, at least once a week. For RNA isolation, the well was washed with PBS before incubation in RLT Plus with β-mercaptoethanol (1/100). For differentiation assays, organoids were passaged and put in culture for 2 d in IntestiCult organoid growth medium and the medium was then changed to IntestiCult organoid differentiation medium (Stem Cell Technologies) supplemented with 2.5 µM DAPT (ab120633; Abcam) for 3 or 5 d for the distal colon and caecum, respectively.

IHC, immunofluorescence and RNAscope

IHC and immunofluorescence were performed following standard protocols. Briefly, fixed samples were dehydrated before embedding in paraffin blocks. Then, 7-µm sections were dewaxed and rehydrated

before antigen retrieval was performed in a pressure cooker using a commercial solution at pH 9 (Dako). Samples were then incubated with hydrogen peroxide to inhibit endogenous peroxidase before being blocked for antibody incubation overnight at 4 °C. The primary antibodies used were rabbit anti-eGFP (2956S; Cell Signaling Technology; 1:200), goat anti-eGFP (Ab6673; Abcam; 1:500), rabbit anti-Ki-67 (MA5-14520; Thermo Fisher Scientific; 1:200), rabbit anti-RFP (600-401-379; Rockland Immunochemicals; 1:2,000), mouse anti-RFP (129244; Abcam; 1:500), mouse anti-β-catenin (610154; BD Transduction Laboratories; 1:250), mouse anti-E-cadherin (610181; BD Transduction Laboratories; 1:500), rabbit anti-Vimentin (ab92547; Abcam; 1:1,000), rabbit anti-α-SMA (MA5-11547; Invitrogen; 1:200), rabbit anti-ChgA (Ab15160; Abcam; 1:200), rabbit anti-Muc2 (PA5-21329; Thermo Fisher Scientific; 1:750), rabbit anti-Dra (NBP1-84450; Novus Biologicals; 1;500), rabbit anti-phospho-MAPK (4370S; Cell Signaling Technology; 1:200) and mouse anti-Trp53 (2524; Cell Signaling Technology; 1:200). For β-catenin IHC, 4-µm sections were collected and antigen retrieval was performed in Tris/EDTA pH 9.0 (ref. 10). On the following day, slides were washed with PBS and incubated with secondary antibodies. For IHC, the secondary antibody used was the peroxidase-conjugated anti-rabbit EnVision+ (Dako) and the staining was amplified by incubating the samples with 3,3′-diaminobenzidine (Dako). For immunofluorescence, the secondary antibodies used were goat anti-rabbit Alexa Fluor 488, goat anti-mouse-Alexa Fluor 647 and donkey anti-goat Alexa Fluor 647 (Invitrogen; 1:500). Samples were counterstained with haematoxylin (for IHC) or DAPI (for immunofluorescence) before mounting for imaging.

RNAscope was performed using a RNAscope 2.5 High-Definition Brown Assay kit (Advanced Cell Diagnostics) following the manufacturer's recommendations. PPIB and DapB RNA probes were used as positive and negative controls, respectively.

Microscopy imaging and analysis. A Zeiss LSM 780 microscope was used to study the immunofluorescence slides. Brightfield images were captured on a Nikon NiE microscope with a DS-Ri2 camera, and stitching features were used. Images were saved as TIFF files and processed using Adobe Photoshop for figure mounting.

Quantitative PCR

FACS-sorted cells were lysed in RLT Plus buffer with β-mercaptoethanol before RNA extraction using an RNeasy Micro kit (Qiagen) according to the manufacturer's instructions. Complementary DNA was generated using a SuperScript III kit (Life Technologies). qPCR was performed in triplicate per gene using SYBR green dye (Promega) according to the manufacturer's instructions, and run on QuantStudio7 qPCR machines (Applied Biosystems). The data were analysed with the ΔΔCt method using QuantStudio 7 software. Ct values were normalized using *Gapdh* housekeeping gene expression. The primer sequences are listed in Supplementary Table 7.

Statistics and reproducibility

For quantification of the traced crypts in the lineage tracing experiments, a minimum of 50 crypts per tissue region (colon proximal, middle, distal or rectum) were counted and the percentages of crypts retaining RFP expression were calculated. One representative section per mouse across three independent tracing experiments was selected for analysis. Mice with the correct genotypes were randomly assigned to control or treated groups. No animals or data points were excluded from the analyses. The data are presented as means ± s.e.m. The data distribution was assumed to be normal, but this was not formally tested. Statistical analyses were performed using GraphPad Prism (GraphPad software). Statistical significance was analysed by paired two-tailed *t*-test. *P* values are indicated in the relevant graphs. Each experiment was repeated at least three times independently. Data collection and analysis were not performed blind to the conditions of the experiments. Precise numbers of replicates are indicated in the figure captions. No statistical method was used to pre-determine sample sizes, but our sample sizes are similar to those reported in previous publications[20,32].

Reporting summary

Further information on research design is available in the Nature Portfolio Reporting Summary linked to this article.

Data availability

Whole colon and small intestine RNA-seq data that support the findings of this study have been deposited in the Gene Expression Omnibus (GEO) under accession code GSE303295. Two-part colon and three-part small intestine RNA-seq data that support the findings of this study have been deposited in the GEO under accession code GSE303433. Colon and small intestine region scRNA-seq data that support the findings of this study have been deposited in the GEO under accession code GSE303434. Previously published pylorus microarray data that were re-analysed here are available from the GEO under accession code GSE121803. Source data are provided with this paper. All other data supporting the findings of this study are available from the corresponding author upon reasonable request.

References

44. Shibata, H. et al. Rapid colorectal adenoma formation initiated by conditional targeting of the *Apc* gene. *Science* **278**, 120–123 (1997).
45. Jonkers, J. et al. Synergistic tumor suppressor activity of BRCA2 and p53 in a conditional mouse model for breast cancer. *Nat. Genet.* **29**, 418–425 (2001).

Acknowledgements

We thank all members of N.B.'s group for technical expertise and insightful discussions; E. Wong for help with generating the mouse lines; S. Mustafah and staff at the A*STAR Singapore Immunology Network Flow Facility for assistance with FACS; staff at the A*STAR Advanced Molecular Pathology Laboratory for pathology evaluation; the A*STAR Microscopy Platform and its staff for assistance with confocal imaging; and E. Cheah and staff at the A*STAR Singapore Bioimaging Consortium–Nikon facility for assistance with brightfield imaging. This study is supported by the A*STAR Institute of Molecular and Cell Biology, National Research Foundation (under NRFI2017-03) and Open Fund Individual Research Grant (OFIRG24Jul-0078).

Author contributions

M.G. designed and performed all of the empirical experiments, collected and analysed the data and wrote the manuscript. S.S., T.C.-Y.C. and S.Y. performed all of the empirical experiments and collected and analysed the data. T.C.-Y.C. performed the mouse husbandry. S.Y. cloned and generated the *Nox1*-2A-eGFP and *Nox1*-2A-CreERT2 mouse lines. S.Y., M.G. and T.C.-Y.C. cloned and generated the *Npy1r*-eGFP-IRES-CreERT2 mouse line. Y.Y. initiated the project and performed the RNA-seq experiment. S.P. and B.L. analysed the RNA-seq and scRNA-seq data and performed the transcriptomics comparison and gene expression analysis. H.Y.G.L. provided critical analyses and wrote the manuscript. N.B. designed and supervised the project, analysed the data and wrote the manuscript. All authors contributed to writing the manuscript.

Competing interests

The authors declare no competing interests.

Additional information

Extended data is available for this paper at https://doi.org/10.1038/s41556-025-01763-1.

Supplementary information The online version contains supplementary material available at https://doi.org/10.1038/s41556-025-01763-1.

Correspondence and requests for materials should be addressed to Nick Barker.

Peer review information *Nature Cell Biology* thanks Louis Vermeulen, Omer Yilmaz and the other, anonymous, reviewer(s) for their contribution to the peer review of this work. Peer reviewer reports are available.

https://doi.org/10.1038/s41556-025-01763-1

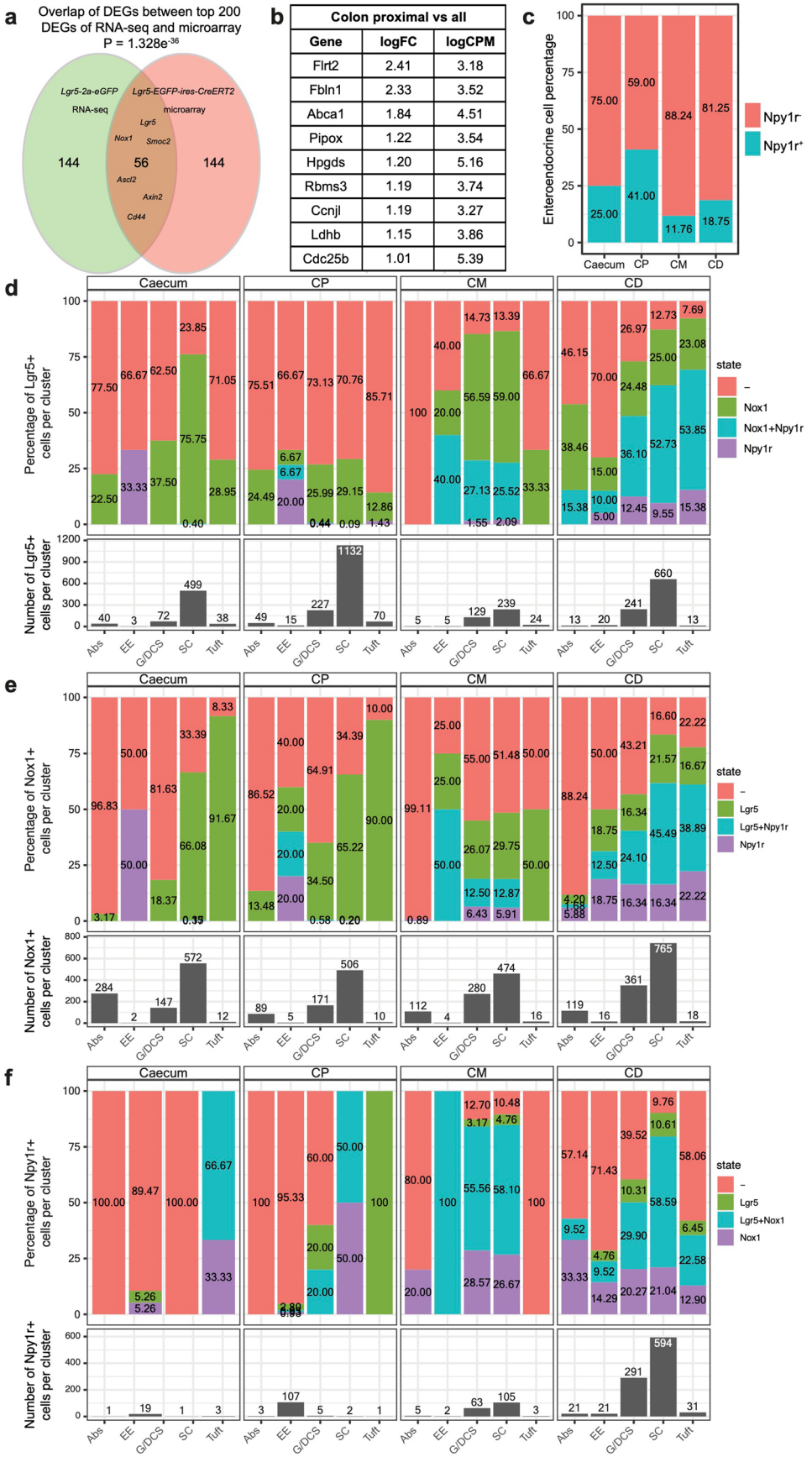

Extended Data Fig. 1 | See next page for caption.

https://doi.org/10.1038/s41556-025-01763-1

Extended Data Fig. 1 | Comparative expression profiling of Lgr5+ stem cell populations along the GI tract identifies novel regional markers. a) Venn diagram representing the overlap between the top 200 differentially expressed genes (DEG) of the Lgr5$^+$ enriched transcriptome using the established *Lgr5-EGFP-IRES-CreERT2* (5KI) mouse and an independent *Lgr5-2A-EGFP* reporter mouse; **b**) Only 9 genes were identified as potentially enriched in proximal colon stem cells. None of these genes could be validated; **c**) Graph representing the percentage of Npy1r$^+$ cells within the enteroendocrine cluster for each tissue compartment; **d**) (Upper panel) Graph representing the percentage of Lgr5$^+$ cells per cluster and their co-expression with Nox1, Npy1r, and both Nox1 and Npy1r; (Lower panel) Graph representing the total number of Lgr5$^+$ cells per cluster; **e**) (Upper panel) Graph representing the percentage of Nox1$^+$ cells per cluster and their co-expression with Lgr5, Npy1r, and both Lgr5 and Npy1r; (Lower panel) Graph representing the total number of Nox1$^+$ cells per cluster; **f**) (Upper panel) Graph representing the percentage of Npy1r$^+$ cells per cluster and their co-expression with Lgr5, Nox1, and both Lgr5 and Nox1; (Lower panel) Graph representing the total number of Npy1r$^+$ cells per cluster.

https://doi.org/10.1038/s41556-025-01763-1

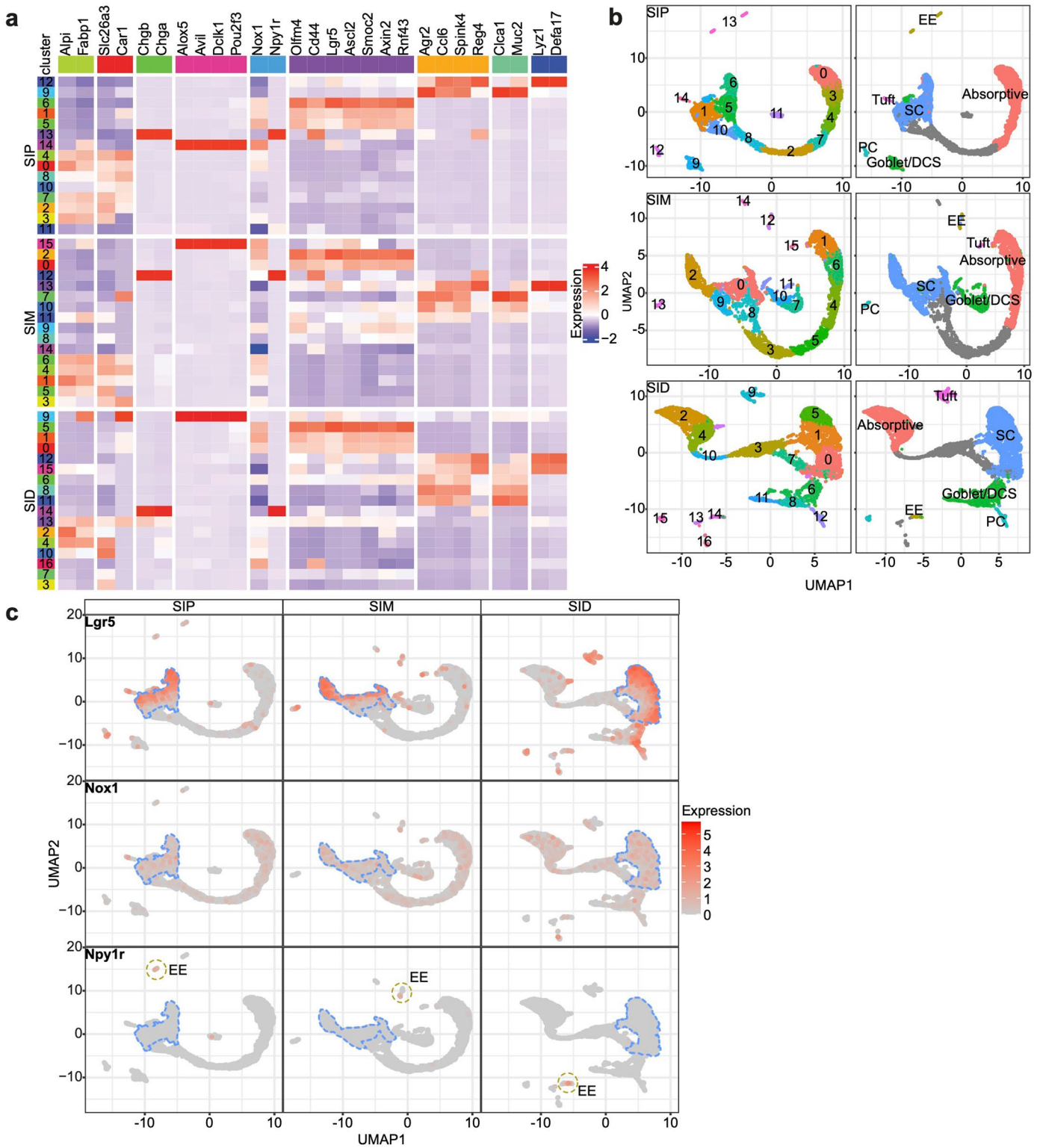

Extended Data Fig. 2 | Nox1 and Npy1r are not enriched in small intestine stem cell clusters. a) Heatmap representing the level of expression of identified key lineage markers for each cluster in the proximal, middle, and distal small intestine; **b**) UMAP plots representing all the clusters identified (left panel) before being reassigned in different lineage clusters using the expression heatmap in a) (right panel); **c**) UMAP plots representing the distribution of Lgr5^{+} (upper panel), Nox1^{+} (middle panel), and Npy1r^{+} cells (lower panel) for each intestinal region (proximal, middle, and distal small intestine). Stem cell (SC) cluster is delineated in blue dashed line and enteroendocrine (EE) cluster is delineated in brown dashed line according to the lineage clusters defined in **b**). Assay was performed on one biological sample per tissue region.

https://doi.org/10.1038/s41556-025-01763-1

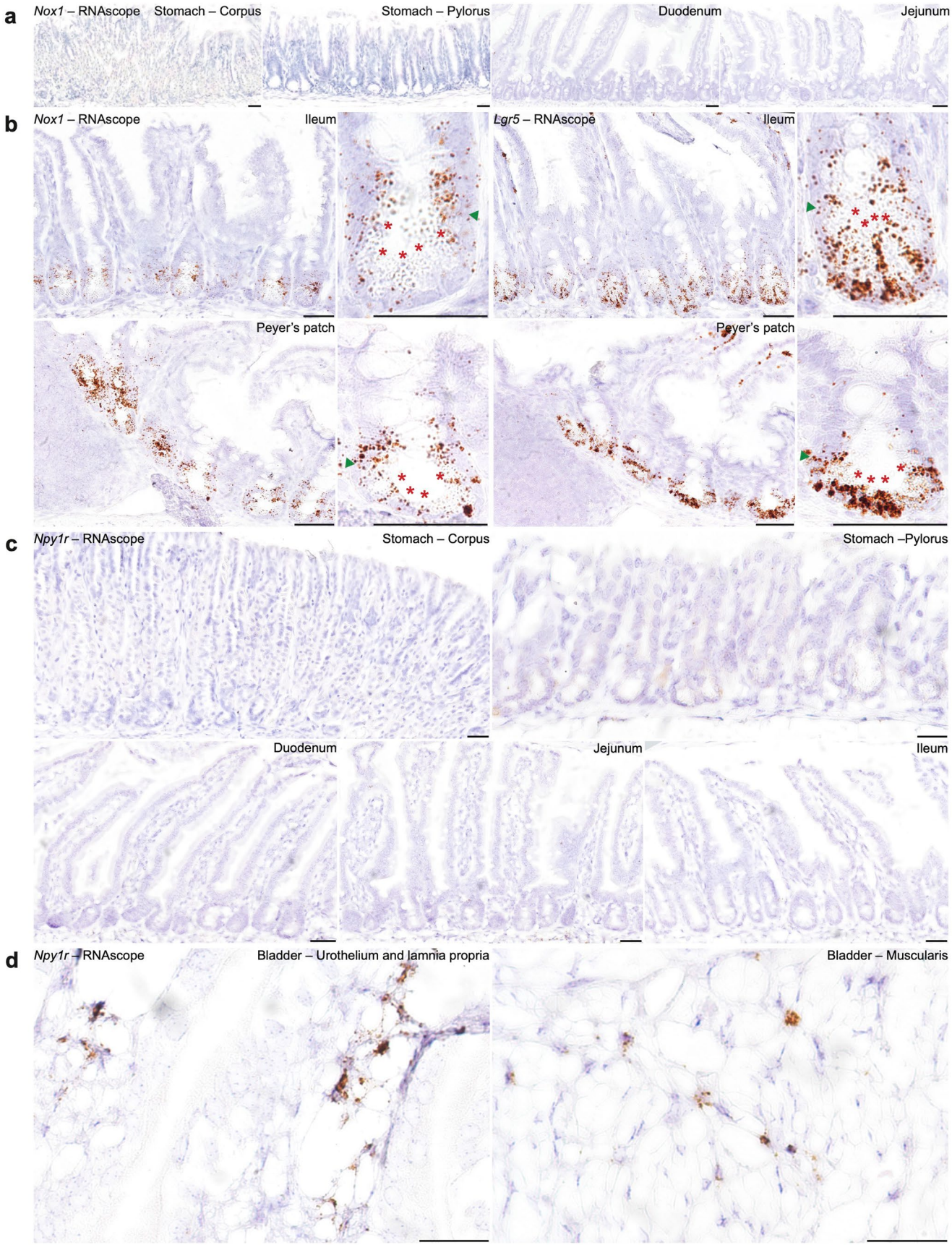

Extended Data Fig. 3 | See next page for caption.

https://doi.org/10.1038/s41556-025-01763-1

Extended Data Fig. 3 | Restricted expression of Nox1 and Npy1r in stem cell/early TA compartments of the Ileum and Peyer's patches of the SI, and in stromal cells of the bladder respectively. a) RNAscope analysis for *Nox1* showed no expression in the stomach (corpus and pylorus) and the proximal part of the small intestine (duodenum and jejunum) (n = 5); **b**) RNAscope analysis for *Nox1* and *Lgr5* showed that *Nox1* was expressed in the early transit-amplifying compartment and lowly expressed in the CBC cells of the ileum. Stronger Nox1 expression primarily in the CBC compartment was detected in intestinal crypts directly adjacent to the Peyer's patches (n = 5). Green arrows indicate the +4 cell position while red stars indicate the CBC cell position; **c**) RNAscope analysis for *Npy1r* showed no expression in the stomach (corpus and pylorus) and the small intestine epithelium (n = 5); **d**) RNAscope analysis of *Npy1r* showed a subset of stromal cells expressing Npy1r in the bladder stroma (n = 5). Scale bar: 25μm.

https://doi.org/10.1038/s41556-025-01763-1

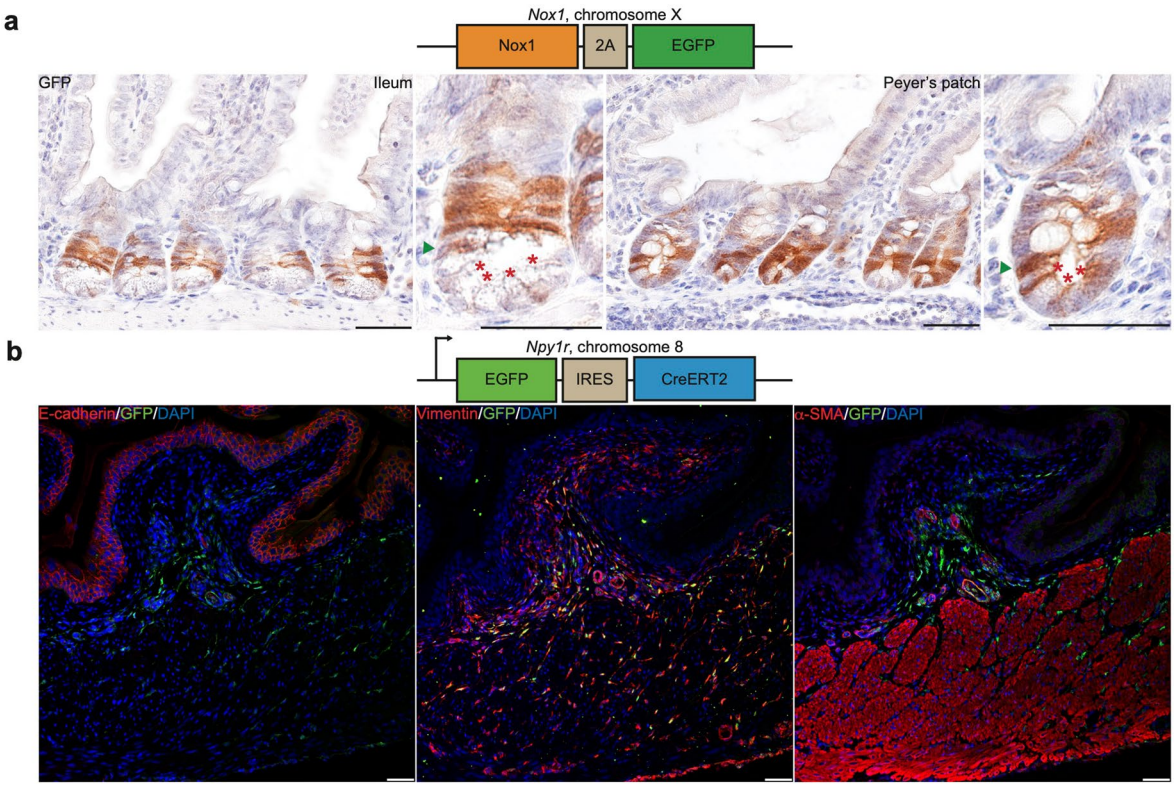

Extended Data Fig. 4 | Nox1- and Npy1r-GFP reporters recapitulate the endogenous expression seen in the small intestine and bladder. a) GFP IHC performed on *Nox1-2A-EGFP* mouse line was observed in the +4 to +6 presumptive TA cells and the CBC cells in the ileum at a lower level. This expression was detected at stronger level in the same cells of the crypt bordering the peyer's patch. Green arrows indicate the +4 cell position while red stars indicate the CBC cell position (n = 5); **b**) Co-IF of GFP with the epithelial marker E-cadherin, the mesenchyme marker Vimentin, and the muscle marker a-SMA showed that GFP^+ cells were $Vimentin^+$ and excluded from the urothelium and muscle cells (n = 5). Scale bar: 25µm (**a**) and 50µm (**b**).

https://doi.org/10.1038/s41556-025-01763-1

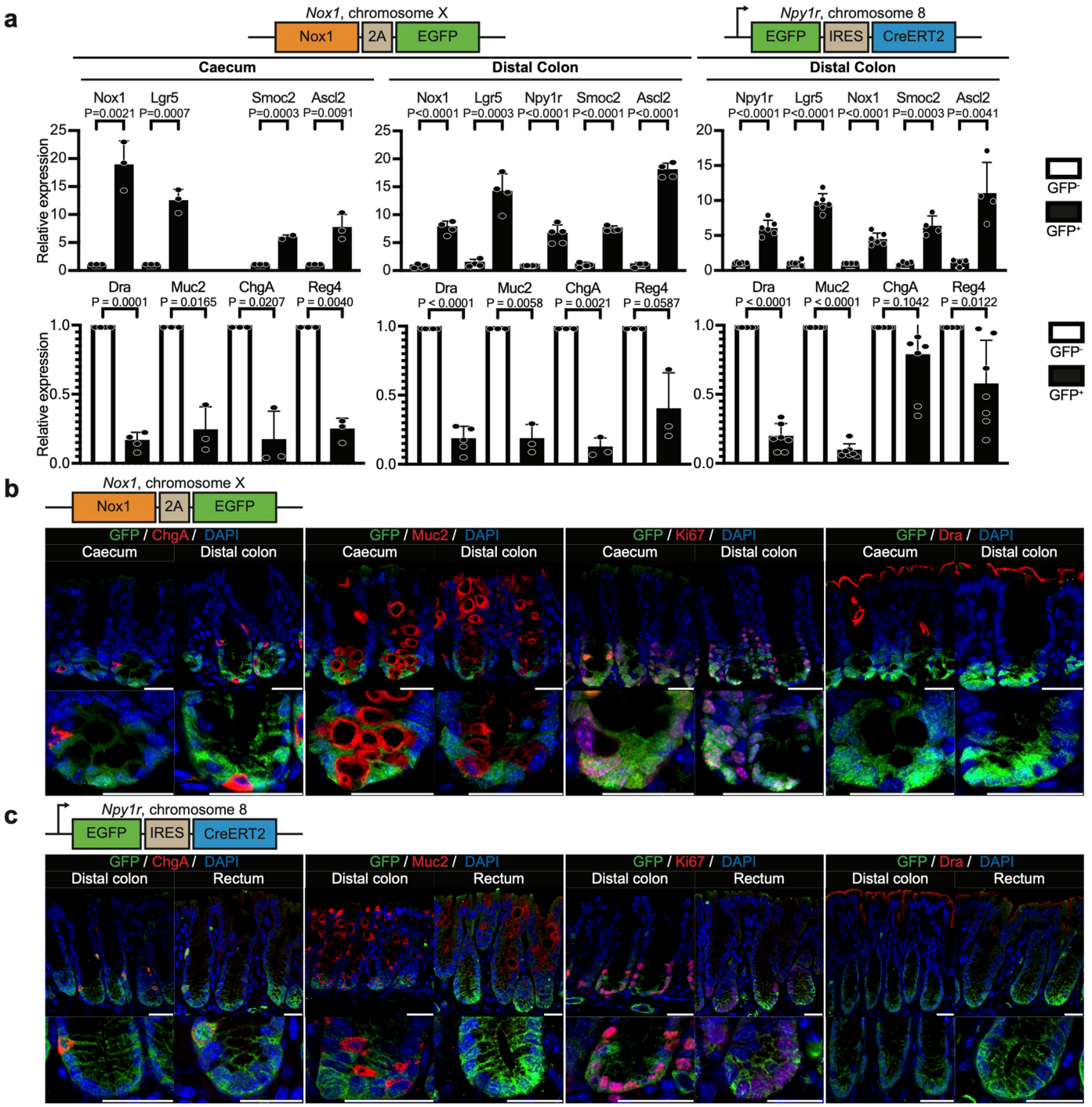

Extended Data Fig. 5 | Nox1+ colon cells express markers of undifferentiated stem cells. a) qPCR analysis on Nox1- and Npy1r-GFP FAC-sorted cells showed an enrichment in stem cell markers Lgr5 (Nox1 caecum n = 3, 12.42 ± 1.219; Nox1 colon n = 4, 14.0825 ± 1.656; Npy1r colon n = 6, 9.6516 ± 0.5590), Smoc2 (Nox1 caecum n = 3, 5.8765 ± 0.2463; Nox1 colon n = 4, 7.5078 ± 0.3144; Npy1r colon n = 4, 6.368 ± 0.7178), Ascl2 (Nox1 caecum n = 3, 7.613 ± 1.399; Nox1 colon n = 4, 17.916 ± 0.7981; Npy1r colon n = 4, 11.0515 ± 2.212) (upper panel). Lineage markers Dra (Nox1 caecum n = 4, 0.079 ± 0.03201; Nox1 colon n = 5, 0.18 ± 0.04231; Npy1r colon n = 7, 0.19 ± 0.03690), Muc2 (Nox1 caecum n = 3, 0.2367 ± 0.09939; Nox1 colon n = 3, 0.18 ± 0.06245; Npy1r colon n = 7, 0.09 ± 0.01952), ChgA (Nox1 caecum n = 3, 0.1667 ± 0.1217; Nox1 colon n = 3, 0.12 ± 0.04041; Npy1r colon n = 7, 0.7814 ± 0.1142), and Reg4 (Nox1 caecum n = 3, 0.15 ± 0.04807; Nox1 colon n = 3, 0.3967 ± 0.1530; Npy1r colon n = 7, 0.57 ± 0.1214) were upregulated in the GFP$^-$ population, indicating that Nox1$^+$ and Npy1r$^+$ cells enrich for stem cells. Statistical significance was determined by two-tailed t-test; **b-c**) Co-IF for GFP and lineage markers using Nox1-2A-EGFP (n = 5) (**b**) and Npy1r-EGFP-IRES-CreERT2 (n = 5) (**c**) mice colon (caecum, distal colon and rectum) showed that GFP$^+$ cells do not overlap with the lineage markers. Co-IF with Ki67 indicated that Nox1$^+$ and Npy1r$^+$ cells are proliferative. Scale bar: 25μm.

https://doi.org/10.1038/s41556-025-01763-1

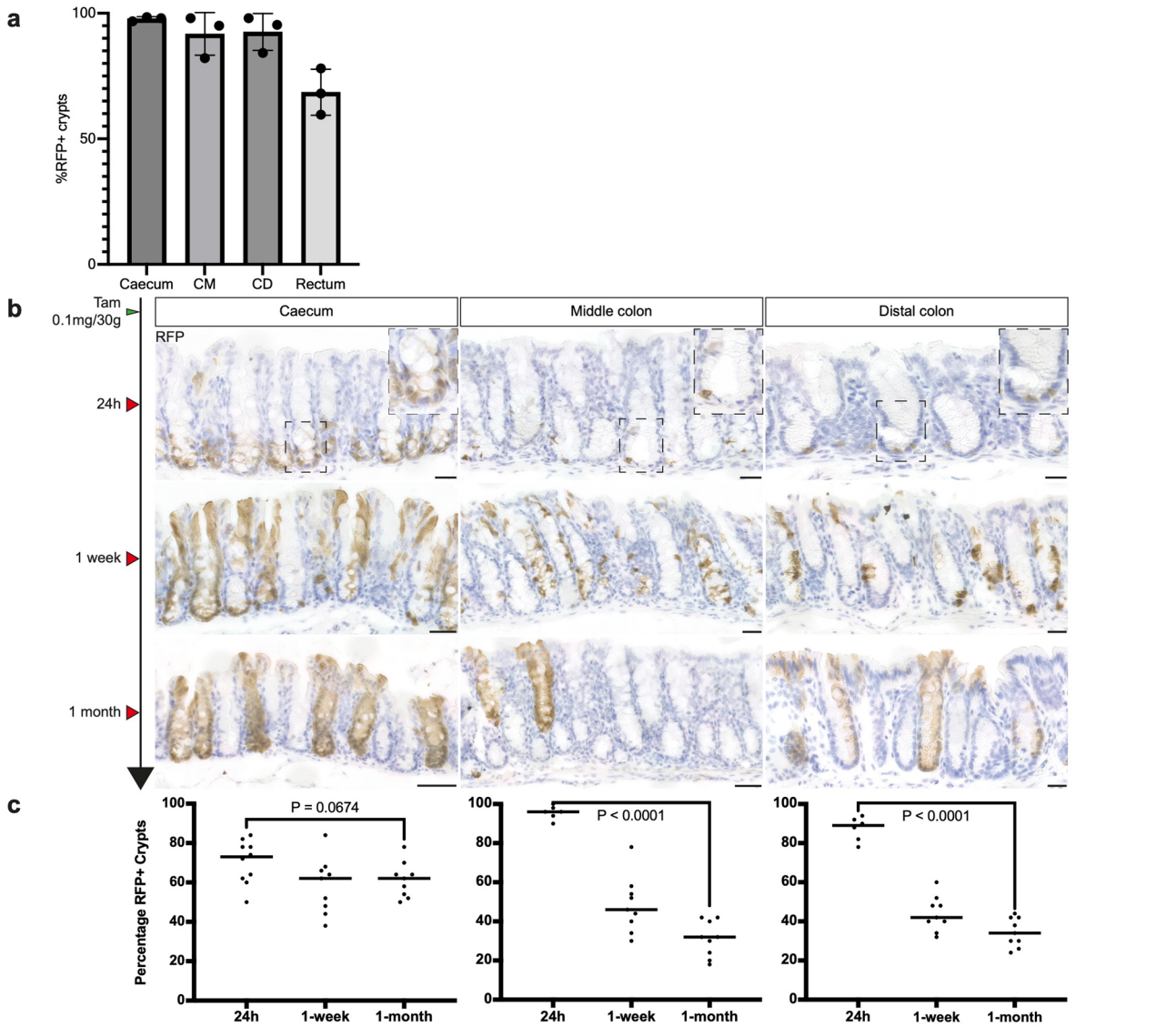

Extended Data Fig. 6 | Nox1-2A-CreERT2 induction is highly efficient in the caecum. a) Graph representing the percentage of crypts retaining the RFP label for each tissue compartment (Caecum: 97.77% ± 0.49%; CM: 91.71% ± 4.86%; CD: 92.53% ± 4.23%; Rectum: 68.54% ± 5.31%; n = 3) at one month post-induction of adult *Nox1-2A-CreERT2, LSL-TdTomato* mice; **b**) Nox1-2A-CreERT2, TdTom mice were injected with 0.1 mg of tamoxifen per 30 g of body weight. Colon compartments were harvested at 24 h, 1-week and 1-month post-induction. At 24 h, all the cells at the base of the caecum crypts were RFP$^+$ while only 1 cell on average was labelled within the middle and distal colon. Insets represent a higher magnification of a representative crypt; After 1-week and 1-month, RFP$^+$ crypt frequency significantly decreased in the middle and distal colon while the RFP$^+$ crypt rate remained constant over time in the caecum (n = 3 mice each); **c**) Quantification of the percentage of RFP+ crypts following 24 h (Caecum n = 10, 70.40% ± 3.47%; Middle colon n = 6, 95.67% ± 1.41%; Distal colon n = 6, 87.33% ± 2.51%), 1 week (Caecum, 58.44% ± 4.75%; Middle colon, 48.44% ± 4.79%; Distal colon, 44.00% ± 2.96%; n = 9) and 1 month (Caecum, 61.33% ± 3.00%; Middle colon, 31.11% ± 3.04%; Distal colon, 34.44% ± 2.47%; n = 9) tracing. Statistical significance was determined by two-tailed t-test. Scale bar: 25µm.

https://doi.org/10.1038/s41556-025-01763-1

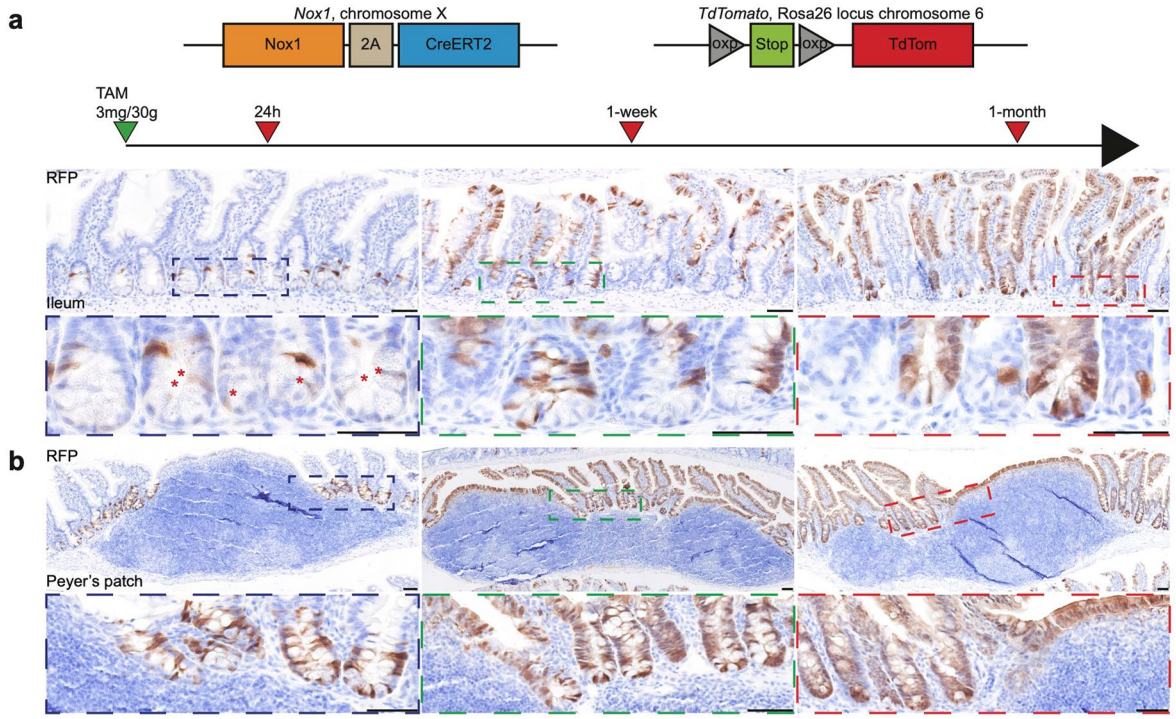

Extended Data Fig. 7 | A subset of Nox1-expressing cells in the small intestine is self-renewing and multipotent. a) *Nox1-2A-CreERT2, Rosa26-LSL-tdTomato* mice were injected with 3 mg/30 g body weight of tamoxifen and harvested after 24 h, 1-week, and 1-month. At 24 h, majority of the cells in the vicinity of the +4 cell were RFP +. Only a small subset of CBC cells were RFP + . After one month of tracing, the crypts and villi in the ileum were partially covered by RFP-expressing cells. Red asterisks represent RFP + CBC cells; **b**) Frequency of RFP^+ cells increased in the crypts adjacent to the Peyer's patches after 24 h induction. All cells within the crypt-villus units adjacent to the Peyer's patches were RFP^+ at 1-month. Scale bar: 25µm.

https://doi.org/10.1038/s41556-025-01763-1

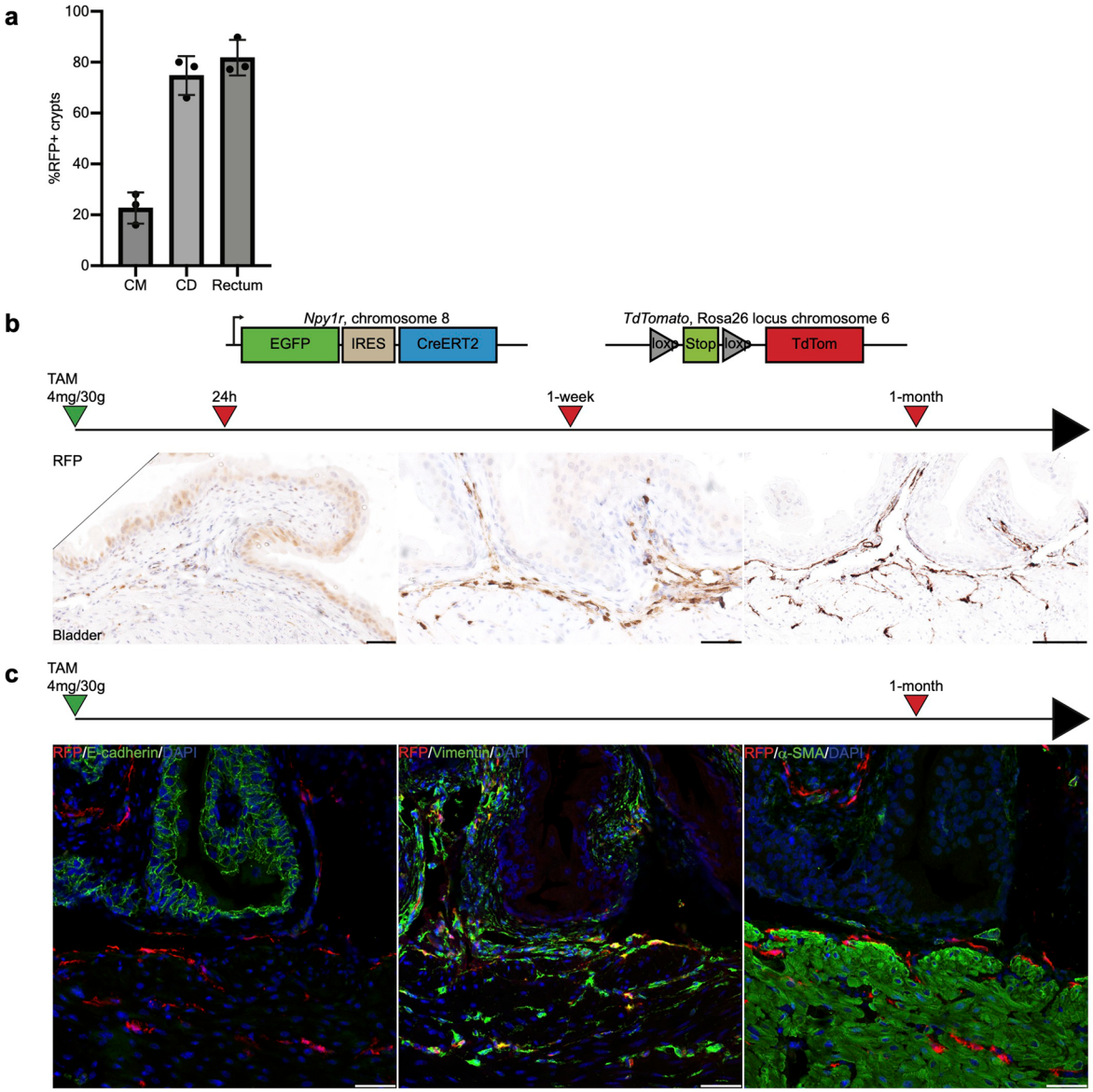

Extended Data Fig. 8 | Npy1r is expressed in long-lived stromal cells of the bladder. a) Graph representing the percentage of crypts retaining the RFP label for each tissue compartment (CM: 22.67% ± 3.53%; CD: 74.79% ± 4.40%; Rectum: 81.79% ± 4.04%; n = 3) at one month post-induction in adult *Npy1r-EGFP-ires-CreERT2, LSL-TdTomato* mice; **b**) *Npy1r- EGFP-ires-CreERT2, Rosa26-LSL-tdTomato* mice were injected with 4 mg/30 g body weight of tamoxifen and harvested after 24 h (n = 3), 1-week (n = 3), and 1-month (n = 3). At 24 h, RFP was detected in stromal cells. This pool of cells was maintained 1 week and 1 month after induction; **c**) Co-IF of RFP with the epithelial marker E-cadherin, the mesenchyme marker Vimentin, and the muscle marker a-SMA showed that RFP$^+$ cells were Vimentin$^+$ and excluded from the urothelium and muscle cells (n = 3). Scale bar: 50µm.

https://doi.org/10.1038/s41556-025-01763-1

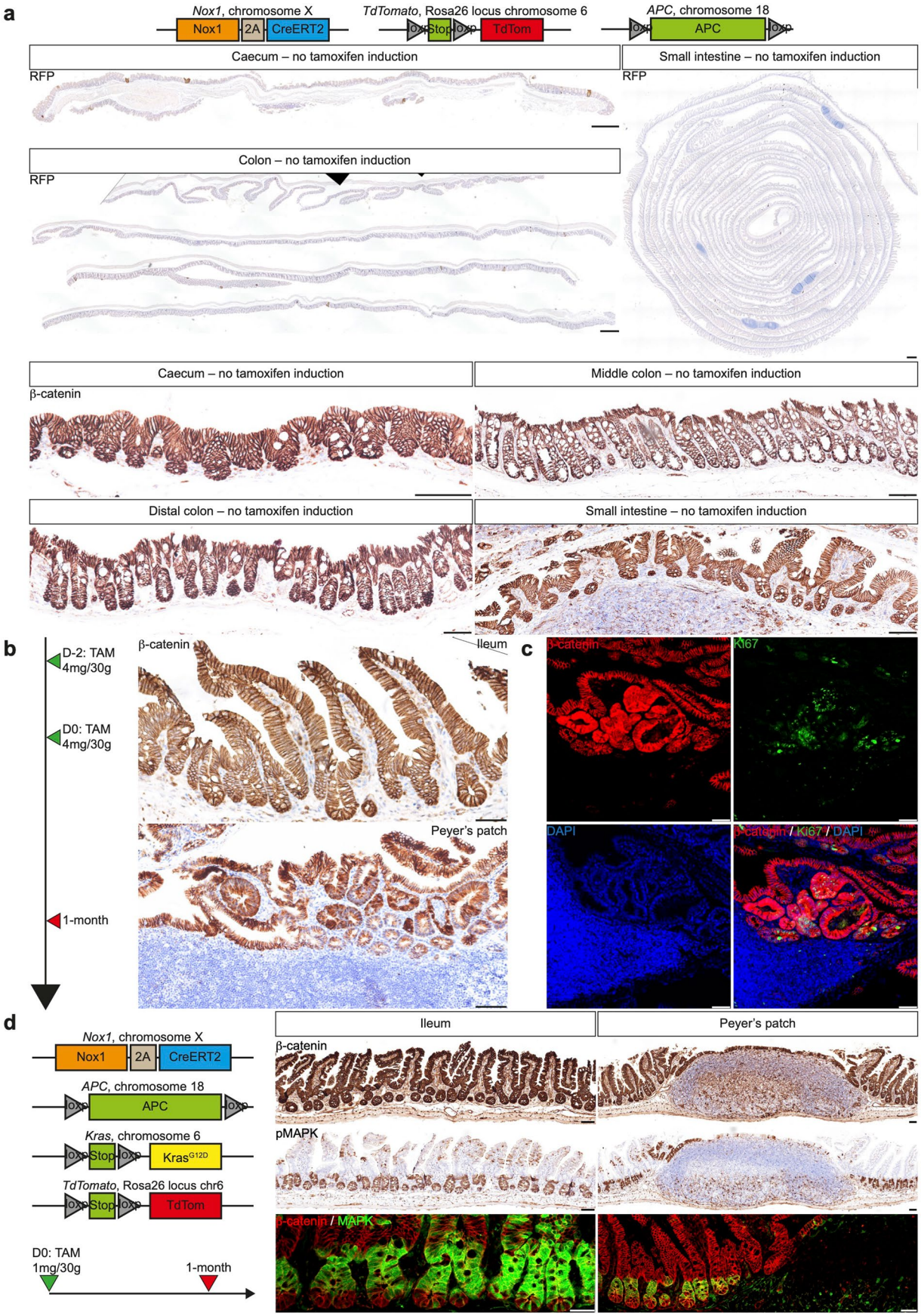

Extended Data Fig. 9 | See next page for caption.

https://doi.org/10.1038/s41556-025-01763-1

Extended Data Fig. 9 | Nox1 CreERT2-driven Apc deletion in the intestine generates mild hyperplasia only in crypts adjacent to Peyer's patches. a) *Nox1-2A-CreERT2, APC*$^{fl/fl}$ 5-month old mice were harvested and stained for RFP and β-catenin in all the digestive tissues expressing *Nox1* to evaluate any potential Cre recombinase expression leakage (n = 3); **b**) Mice were injected twice at 2-days interval with 4 mg/30 g body weight of tamoxifen and the small intestine harvested after 1 month. β-catenin IHC showed nucleocytoplasmic accumulation only in the crypts directly adjacent to Peyer's patches but absent from the ileum (n = 4); **c**) Co-IF of β-catenin with Ki67 showed that these hyperplastic crypts were proliferative (n = 4); **d**) *Nox1-2A-CreERT2, APC*$^{fl/fl}$ mice were bred with *LSL-Kras*^{G12D} mice. Mice were induced with 1 mg of tamoxifen per 30 g of body weight and harvested after 1 month. No β-catenin accumulation was detected in the ileum and Peyer's patch epithelium and hyperactivation of pMapk was found as expected in the CBC and TA cells (n = 3). Scale bar: 250μm (**a**, upper panel), 50μm (**a**, lower panel), and 25μm (**b**-**d**).

https://doi.org/10.1038/s41556-025-01763-1

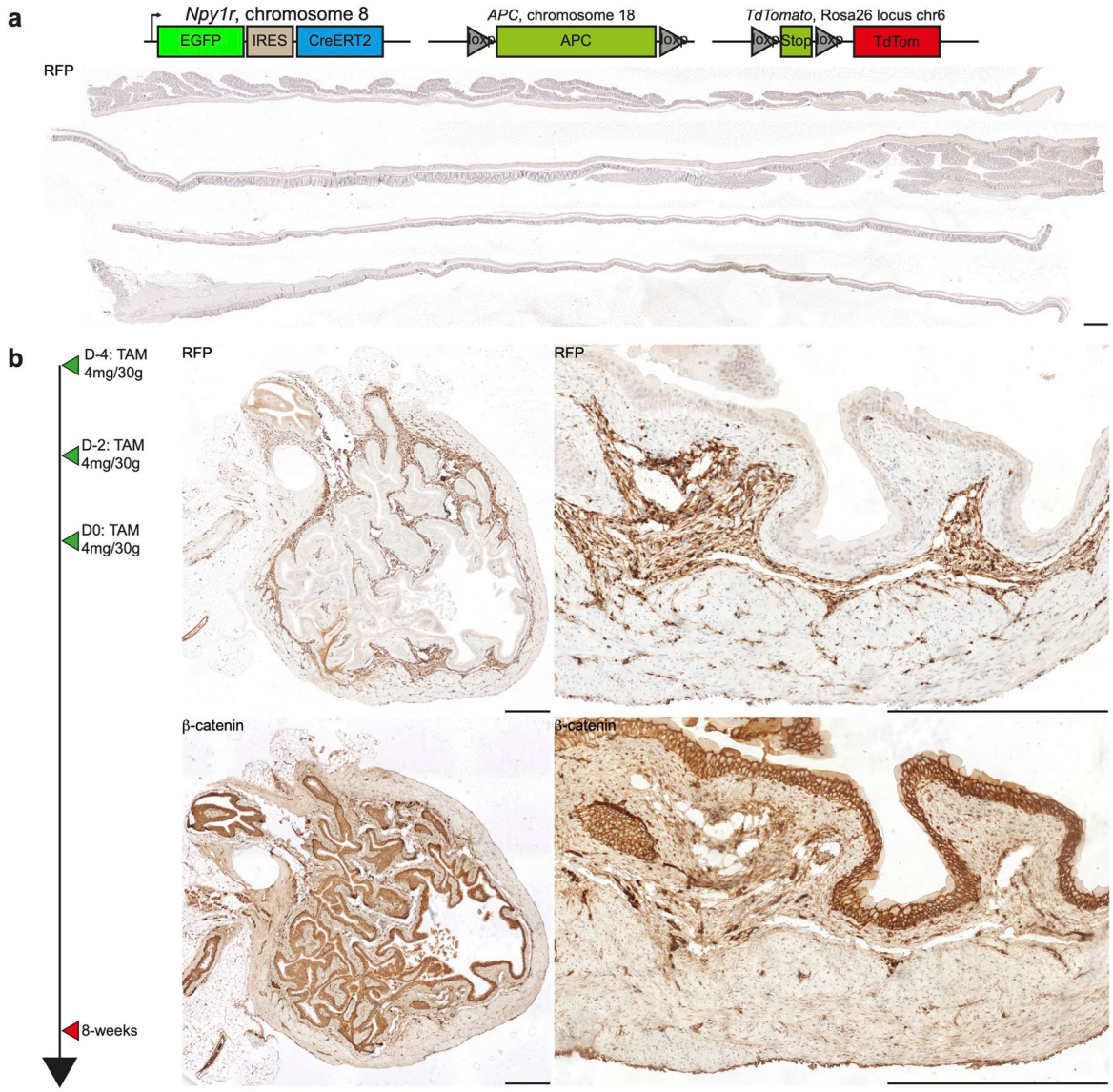

Extended Data Fig. 10 | Npy1r CreERT2-driven Apc deletion does not initiate tumour formation in the bladder. a) 3-month old *Npy1r-EGFP-IRES-CreERT2, APC$^{fl/fl}$* mice were harvested and stained for RFP in the entire colorectum to evaluate any potential Cre recombinase expression leakage. No RFP staining was detected (n = 3); **b**) *Npy1r-EGFP-IRES-CreERT2, APC$^{fl/fl}$* mice were injected with 3 doses of 4 mg tamoxifen per 30 g body weight every 2 days and harvested 8 weeks post- induction. No β-catenin accumulation was detected in the bladder (n = 6). Scale bar: 500 μm.

nature portfolio

Corresponding author(s): Nick Barker

Last updated by author(s): Jul 24, 2025

Reporting Summary

Nature Portfolio wishes to improve the reproducibility of the work that we publish. This form provides structure for consistency and transparency in reporting. For further information on Nature Portfolio policies, see our Editorial Policies and the Editorial Policy Checklist.

Statistics

For all statistical analyses, confirm that the following items are present in the figure legend, table legend, main text, or Methods section.

n/a	Confirmed
☐	☒ The exact sample size (*n*) for each experimental group/condition, given as a discrete number and unit of measurement
☒	☐ A statement on whether measurements were taken from distinct samples or whether the same sample was measured repeatedly
☐	☒ The statistical test(s) used AND whether they are one- or two-sided *Only common tests should be described solely by name; describe more complex techniques in the Methods section.*
☒	☐ A description of all covariates tested
☒	☐ A description of any assumptions or corrections, such as tests of normality and adjustment for multiple comparisons
☐	☒ A full description of the statistical parameters including central tendency (e.g. means) or other basic estimates (e.g. regression coefficient) AND variation (e.g. standard deviation) or associated estimates of uncertainty (e.g. confidence intervals)
☐	☒ For null hypothesis testing, the test statistic (e.g. *F*, *t*, *r*) with confidence intervals, effect sizes, degrees of freedom and *P* value noted *Give P values as exact values whenever suitable.*
☒	☐ For Bayesian analysis, information on the choice of priors and Markov chain Monte Carlo settings
☒	☐ For hierarchical and complex designs, identification of the appropriate level for tests and full reporting of outcomes
☒	☐ Estimates of effect sizes (e.g. Cohen's *d*, Pearson's *r*), indicating how they were calculated

Our web collection on statistics for biologists contains articles on many of the points above.

Software and code

Policy information about availability of computer code

Data collection	BD FACS software sorter software (v1.1), QuantStudio Real-Time PCR software (v1.3) Nikon NIS-Elements AR (v5.11), Zeiss ZEN black, Cell Ranger 7.1.0 (10X genomics)
Data analysis	Fiji (ImageJ2 v2.14.0/1.54f), GraphPad Prism (v10.1.1) edgeR (v4.2.1), FindAllMarkers function in the Seurat package.

For manuscripts utilizing custom algorithms or software that are central to the research but not yet described in published literature, software must be made available to editors and reviewers. We strongly encourage code deposition in a community repository (e.g. GitHub). See the Nature Portfolio guidelines for submitting code & software for further information.

Data

Policy information about availability of data

All manuscripts must include a data availability statement. This statement should provide the following information, where applicable:

- Accession codes, unique identifiers, or web links for publicly available datasets
- A description of any restrictions on data availability
- For clinical datasets or third party data, please ensure that the statement adheres to our policy

The datasets generated during and/or analysed during the current study will be made available in the GEO repository. Source data for Fig.4 and Extended data Fig.5, 6 and 8 are provided with this study. All other data supporting the findings of this study are available from the corresponding author on reasonable request.

Research involving human participants, their data, or biological material

Policy information about studies with human participants or human data. See also policy information about sex, gender (identity/presentation), and sexual orientation and race, ethnicity and racism.

Reporting on sex and gender	N/A
Reporting on race, ethnicity, or other socially relevant groupings	N/A
Population characteristics	N/A
Recruitment	N/A
Ethics oversight	N/A

Note that full information on the approval of the study protocol must also be provided in the manuscript.

Field-specific reporting

Please select the one below that is the best fit for your research. If you are not sure, read the appropriate sections before making your selection.

☒ Life sciences ☐ Behavioural & social sciences ☐ Ecological, evolutionary & environmental sciences

For a reference copy of the document with all sections, see nature.com/documents/nr-reporting-summary-flat.pdf

Life sciences study design

All studies must disclose on these points even when the disclosure is negative.

Sample size	No sample size calculation was performed. All qualitative experiments (e.g. immunostaining) were done with at least three biological replicates with all showing the same outcome, indicating applicability to the broader sample. We included as many independent replicates as possible (3 or more) in quantitative experiments, and used statistical tests to determine if any observable difference was statistically significant. Sample size is deemed sufficient with a statistically significant difference.
Data exclusions	In principle, data were only excluded for failed experiment resulting from technical error.
Replication	We performed experiments on at least 3 biological replicates to ensure reproducibility of results.
Randomization	No randomisation of mice. Mice analysed were litter mates and sex-matched whenever possible.
Blinding	Investigators were not blinded to mouse genotypes. Data reported for mouse experiments are not subjective but based on experimental observations.

Reporting for specific materials, systems and methods

We require information from authors about some types of materials, experimental systems and methods used in many studies. Here, indicate whether each material, system or method listed is relevant to your study. If you are not sure if a list item applies to your research, read the appropriate section before selecting a response.

Materials & experimental systems

n/a	Involved in the study
☐	☒ Antibodies
☒	☐ Eukaryotic cell lines
☒	☐ Palaeontology and archaeology
☐	☒ Animals and other organisms
☒	☐ Clinical data
☒	☐ Dual use research of concern
☒	☐ Plants

Methods

n/a	Involved in the study
☒	☐ ChIP-seq
☐	☒ Flow cytometry
☒	☐ MRI-based neuroimaging

Antibodies

Antibodies used	rabbit anti-EGFP (1:200; Cell Signalling, 2956S), goat anti-EGFP (1:500, Abcam, Ab6673), rabbit anti-KI67 (1:200; Thermofisher,

Antibodies used	MA5-14520), rabbit anti-RFP (1:2000; Rockland, 600-401-379), mouse anti-RFP (1:500, Abcam, 129244), mouse anti-⊡-catenin (1:250, BD Transduction Laboratories, 610154), mouse anti-E-cadherin (1:500; BD Transduction, 610181), rabbit anti-Vimentin (1:1000; Abcam, ab92547), rabbit anti ⊡-SMA (1:200; Invitrogen, MA5-11547), rabbit anti-ChgA (1:200, Abcam, Ab15160), rabbit anti-Muc2 (1:750,Thermo Fisher Scientific, PA5-21329), and rabbit anti-Dra (1;500, Novus biologicals, NBP1-84450); rabbit anti-Trp53 (1:200; Cell Signaling; 2524); Rabbit anti-phopho-MAPK (Cell Signaling, 4370S)
Validation	The antibodies were validated by the relevant companies and show expected staining patterns and cellular localisation in our experiments. The requested details are summarised in the methods section.

Animals and other research organisms

Policy information about studies involving animals; ARRIVE guidelines recommended for reporting animal research, and Sex and Gender in Research

Laboratory animals	Adult B6 mice (6 weeks or older) of both genders were used in the study. All animal experiments were approved by the Institutional Animal Care and Use Committee of Singapore (IACUC 231777). All animals were placed under a 12-h light–dark cycle. Room temperature was maintained at 21 ± 1 °C with 55–70% humidity. All mice were bred and maintained under specific-pathogen-free conditions in individually ventilated cages.
Wild animals	The study did not involved wild animals.
Reporting on sex	No sex segregation has been applied for this study. Only male animal were used for cell dissociation and sorting due to better observed cell viability following tissue processing.
Field-collected samples	The study did not involved samples collected in the field.
Ethics oversight	All experiments involving animals were approved by Institutional Animal Care and Use Committee of Singapore.

Note that full information on the approval of the study protocol must also be provided in the manuscript.

Plants

Seed stocks	N/A
Novel plant genotypes	N/A
Authentication	N/A

Flow Cytometry

Plots

Confirm that:

☒ The axis labels state the marker and fluorochrome used (e.g. CD4-FITC).

☒ The axis scales are clearly visible. Include numbers along axes only for bottom left plot of group (a 'group' is an analysis of identical markers).

☒ All plots are contour plots with outliers or pseudocolor plots.

☒ A numerical value for number of cells or percentage (with statistics) is provided.

Methodology

Sample preparation	Mouse small intestine, colorectal or caecum tissues were incubated in chelation buffer (5.6 mM sodium phosphate, 8 mM potassium phosphate, 96.2 mM sodium chloride, 1.6 mM potassium chloride, 43.4 mM sucrose, 54.9 mM d-sorbitol in milliQ water) with 10 mM (colorectum and caecum) or 2 mM (small intestine) EDTA, 1 mM dithiothreitol (DTT) and 1 mM N-acetylcysteine (NAC) for 2h (colorectum and caecum) or 45 minutes (small intestine) at 4 ºC on a roller. Glands were isolated by repeated pipetting of finely chopped tissue in cold chelation buffer. Chelation buffer containing isolated glands was filtered through a 100 µm filter mesh, and centrifuged at 720g at 4 ºC for 3 min. The pellet was resuspended in TrypLE (Life Technologies) with DNaseI (0.8 U/µl) (Sigma) and incubated at 37 °C for 10 min with intermittent trituration for digestion into single cells. Digestion was quenched by dilution with cold HBSS buffer. The suspension was centrifuged at 720g at 4 °C for 3 min. The pellet was resuspended in 2% Fetal Bovine Serum (FBS, colorectum and caecum) or 20% FBS + 5mM EDTA and filtered through the 4 ⊡m filter mesh cap of the FACS tube. Before sorting, DAPI was added at a final concentration of 1⊡g/ml to stain dead cells. Single cells were sorted on BD Influx Cell Sorter (BDBiosciences). Cells were collected in RLTPlus buffer

	(Qiagen) supplemented with β-mercaptoethanol (1/100) for RNA extraction or advanced DMEM:F12 medium (Gibco) supplemented with 0.5% Matrigel (Corning) for organoid culture.
Instrument	BD Influx
Software	BD FACSDiva for collection and population analysis
Cell population abundance	Sort with GFP-reporter mice required 1 small intestine separated in 3 parts, 4 colon separated in 2 parts and 1 caecum per sample. Depending of the marker (LGr5, Nox1 or Npy1r) and the tissue, a range of 10000 to 50000 positive cells per experiment were collected. Negative population is always in abundance. Cell populations collected were subsequently confirmed by qPCR.
Gating strategy	Positive/Negative gating strategy was defined with wild type or unstained cells, and subsequently confirmed by qPCR.

☒ Tick this box to confirm that a figure exemplifying the gating strategy is provided in the Supplementary Information.